Prompt Neutrino Production

In the 1982 Beam Dump Experiment at CERN

Paul Bostock

Jesus College

Thesis submitted for the degree of
Doctor of Philosophy in the University of Oxford

July 1985

Prompt Neutrino Production

In the 1982 Beam Dump Experiment at CERN

Paul Bostock

Jesus College

Abstract

Principles of beam dump experiments are reviewed and the 1982 beam dump at CERN using the Big European Bubble Chamber is described in detail. Neutrino events have been detected using both the bubble chamber and its associated electronic detectors. Prompt event rates are established for ν_μ, $\bar{\nu}_\mu$, ν_e and $\bar{\nu}_e$. The prompt rates are consistent with lepton universality. The charm production cross-section required to explain the prompt electron-(anti)neutrino signal is approximately 16–105 μb per nucleon, assuming linear dependence of this cross-section on nucleon number. This range of values reflects the fact that we have not been able to find a model which is consistent with all aspects of the data.

The neutral to charged current ratio for electron-neutrinos is found to be 0.23 ± 0.16. The expected number of tau-neutrino events is estimated and kinematic and visual searches for tau-neutrino interactions are described. One visually detected candidate is described in detail. No positive evidence for a tau-neutrino interaction has been found. From the ratio of neutral to charged current events in the data we infer that no more than 4% of the prompt charged current events and 40% of the total prompt signal may be attributed to tau-neutrinos at 90% CL.

Thesis submitted for the degree of
Doctor of Philosophy in the University of Oxford

July 1985

To my family

Acknowledgements

I would like to thank Gerald Myatt for all his help, advice and patience as my supervisor.

I also thank Per–Olof Hulth, Jon Guy, Hans Klein, Jelena Krstić, Madjid Mobayyen, Andy Parker, Wilbur Venus and Horst Wachsmuth with whom I have enjoyed working on various aspects of the experiment, Gino Saitta, who was an entertaining trainer for EMI shifts and Mike Bowler, Steve Colwill, Gerard Corrigan and Louis Lyons for helpful advice on some physics problems.

I am grateful to many people in the department who have helped in a variety of ways—particularly Willie Black and Nick West; Sue Collier, Penny Gledhill and Daphne Pollard; Diane, Edna, Helen, Paul and Robin who all helped with special scanning jobs; the photographic department and drawing office, Pat and Betty in the tape library and Dominic and Keith in Stores. I am grateful also to the staff at Jesus College, who made it an enjoyable place to belong, and to Mrs. Gibbons for making me very welcome at her house this year.

I thank all the people who have kept me company over the last 12 terms, especially my former flatmates Clare and Laurie; Andy, Anne, Chris, Edna, Gerard, Kevin, Neil, Nick, Paul Dauncey, Paul Shotton, Phil Allport, Phil Bull, Sarah, Simon, Steve and Sue.

I am very grateful to my family for their help, support and amusing letters over the years, and to my father also for binding the theses.

I acknowledge the financial support of the SERC during the first three years and Jesus College for a grant for this last term.

A spirit in my feet
Hath led me—who knows how?
To thy chamber window, sweet!

P.B.Shelley

Contents

1

Beam Dump Experiments

This chapter sets out the general principles of beam dump experiments and, with a brief review of previous beam dump results, provides a context for the current experiment.

1.1 Introduction to Beam Dump Experiments

In keeping with the spirit of high energy physics, the motivation for 'beam dump' experiments is to discover new particles and new effects. The term 'beam dump' refers to the established experimental arrangement for such a search, in which an intense beam of high energy protons is absorbed in a thick, dense target—the dump; contrasting this with a 'conventional' layout leads us to a clearer idea of what we should be looking for. Conventional fixed target experiments typically use a primary proton beam incident on a target of low effective density and study the interactions of the outgoing hadronic particles— largely pions and kaons—and their decay products, muons and muon-neutrinos. Any other processes, such as the production of heavy flavour particles, heavy leptons and their neutrinos, supersymmetric particles and so on are negligible in rate in these experiments and for this reason a complementary set up is required.

Beam dump experiments are able to search for particles produced with small cross sections in proton – target-nucleus collisions. In particular they are sensitive to short lived particles whose decay modes include neutrinos in the final state. Neutrinos from such sources are called 'prompt'. The essential principle of the experiment is a simple one: particles which are sources of neutrinos must decay in the dump rather than be absorbed. For particles whose lifetime is $\gamma\tau_p$ and which have an absorption length λ in the target, the fraction f which decay is given by

$$f = \frac{\lambda}{\lambda + \gamma\tau_p}.$$

For pions and kaons, $\gamma\tau_p \gg \lambda$ and the rate of decays is proportional to the absorption length, and hence inversely proportional to target density. For short lived particles, with lifetimes of the order of 10^{-11} s or less, $\gamma\tau_p \ll \lambda$, and the rate is independent of target density. If the decay rate is plotted against inverse target density we expect a straight line with a constant component (the prompt rate) and a linearly increasing term (the conventional rate). To summarise, we should expect the following contributions to the flux of particles emerging from the dump and reaching the detector:

(i) 'Conventional' neutrinos from decays of pions and kaons. The parents are produced with large cross section but are attenuated by absorption in the target by an energy dependent factor of the order of 10^{-3}–10^{-4}, so that the contribution to the neutrino flux is comparable with . . .

(ii) 'Prompt' neutrinos from the comparatively small number of short-lived particles produced, but whose lifetime is small enough to prevent significant absorption in the target.

(iii) Other penetrating particles—we might also expect particles to emerge if they have have long absorption lengths. Such particles would not interact strongly, and their production cross-sections in the proton interactions must be small. Nevertheless, this category includes some interesting possibilities such as axions, gluinos, new neutrinos and so on. These sources of particles would contribute to the prompt flux.

(iv) Lastly, there is a background from interactions of beam protons outside the target, and this must be minimised if the results are to be of any significance. The instrumentation required to monitor the interactions of beam protons before they reach the target is decribed in section 2.2.

1.2 Previous Beam Dump Experiments

The first two beam dump runs with 400 GeV protons were performed at CERN in 1977 and 1979. In these experiments the dump was some 415m further from the detectors than in its 1982 position. During the 1977 run, 3.5×10^{17} protons were dumped on a full density target. The effects of scraping and so on were measured by deliberate mis-steering of the beam and a section of the run was dedicated to measuring the cosmic-ray background. The bubble chamber groups (Gargamelle, BEBC) reported an excess of electron-neutrino events above the expected background [1,2], for which the most plausible explanation was the production and subsequent semileptonic decay of charmed hadrons in the dump with a cross section of the order of a few hundred μb per nucleon. The CDHS counter detector recorded an excess of muon-neutrino events as well as electron-neutrinos [3]. These experiments were the first to see evidence for hadronic charm production.

Having demonstrated that the idea worked the 1979 run was performed in order to measure the prompt rates with more accuracy and control. A one-third density target was used so that rates could be extracted by extrapolation as well as by background subtraction and eight ionisation monitors were installed to measure beam scraping. More protons were delivered to the targets and the three groups reported significant prompt rates with the ratio of prompt $e^{\pm}$ to prompt $\mu^{\pm}$ less than one,[4–6] a result which conflicts with e–μ universality and for which there is no simple explanation in terms of established theory. The CDHS measurement of $\bar{\nu}$: ν implies a baryonic contribution to the charm cross section. The CHARM collaboration also reported an excess of prompt neutral interactions at low energy (2–20 GeV), which was not observed by the other groups.

The inequality of the electron- and muon-neutrino fluxes was a sufficiently interesting observation to merit further study with improved statistics. The beam dump target was moved significantly closer to the detectors, further scraping monitors were installed and more protons were delivered to the target. The possibility of searching for a tau-neutrino interaction visually in BEBC was also anticipated, and the bubble chamber was equipped with a high resolution camera. A summary is presented in table 1.1

Table 1.1 Summary of Previous Beam Dump Experiments

Year	Detector Mass, L	Protons $/10^{17}$	Target	New results
1977	BEBC 13t, 820m	3.5	$\frac{1}{1}$	Prompt $e^{\pm}$ signals: 11 e^- (expect 1.8 ± 0.4) 4 e^+ (expect 0.5 ± 0.25)
1977	CDHS 492t, 890m	4.3	$\frac{1}{1}$	Prompt $e^{\pm}$ $\mu^{\pm}$ signals: 180 ± 74 μ^-, 78 ± 34 μ^+ 104 ± 18 e^-, 50 ± 9 e^+
1977	GGM 10.5t, 950m	3.5	$\frac{1}{1}$	Prompt $e^{\pm}$ signal 8.9 CC $e^{\pm}$ (expect 1.1)
1979	BEBC 13.5t, 820m	7.7 3.1	$\frac{1}{1}$ $\frac{1}{3}$	$e : \mu = 0.59 \pm {}^{.85}_{.29}$ $N_{\tau} < 10\% \ N_{prompt}$
1979	CDHS 492t, 890m	6.6 2.5	$\frac{1}{1}$ $\frac{1}{3}$	$\bar{\nu}_{\mu} : \nu_{\mu} = 0.46 \pm {}^{.21}_{.16}$ $e : \mu = 0.64 \pm {}^{.25}_{.15}$ no excess 0μ events
1979	CHARM 100t, 910m	7.0 2.6	$\frac{1}{1}$ $\frac{1}{3}$	$e : \mu = 0.48 \pm .12 \pm .10$ $\bar{\nu}_{\mu} : \nu_{\mu} = 1.3 \pm {}^{.6}_{.5}$ $54 \pm 19 \pm 9$ excess 0μ events
1982	BEBC 11.5t, 406m	19.1 8.1	$\frac{1}{1}$ $\frac{1}{3}$	This experiment, results—chapters 3,4

References

[1] P.Alibran et. al., *Physics Letters* **74B** (1978) 134.

[2] P.C.Bosetti et. al., *Physics Letters* **74B** (1978) 143.

[3] T.Hansl et. al., *Physics letters* **74B** (1978) 139.

[4] P.Fritze et. al., *Physics Letters* **96B** (1980) 427.

[5] M.Jonker et. al., *Physics Letters* **96B** (1980) 435.

[6] H.Abramowicz et. al., *Zeitschrift für Physik* **C13** (1982) 179.

2

Experimental Details

The experimental arrangement and the data processing procedure used by the WA66 collaboration for the 1982 beam dump run are described, showing how the principles introduced in the previous chapter are put into practice.

2.1 General Description

The layout of the experiment is shown (figure 2.1). This choice of arrangement, requiring the intense proton beam incident on the dump and a massive detector downstream, is dictated by the smallness of the cross-sections for producing prompt neutrinos and for their subsequent reinteraction. Roughly 10^{15} protons are delivered to the dump per event detected. The proton beam, the dump and the detectors will be described first, followed by the off-line procedure which was used to identify neutrino interactions and to obtain as complete a description of them as possible.

2.2 The Beamline

The experiment requires a large number of protons at the highest available energy to be delivered to the dump under controlled conditions. The source of the protons is the CERN SPS system, which ejects protons with a mean momentum of 400 GeV into the beamline every $12\,s$. Under stable running conditions, one beam pulse of around 10^{13} protons is ejected in a fast spill of $23\,\mu s$—the time it takes a proton to go round the SPS ring once. In order to normalise the rates on different targets, the proton flux is measured by a set of three beam-current transformers which each have a resolution of 10^{10} protons and an accuracy of 0.2%.[1] It is essential that there are no interactions between the proton beam and the vacuum pipe walls; these interactions ('scraping') would produce neutrino secondaries at a rate independent of target, faking a prompt signal. Such a background must be kept to a minimum. To monitor possible proton losses, 26 ionisation chambers were

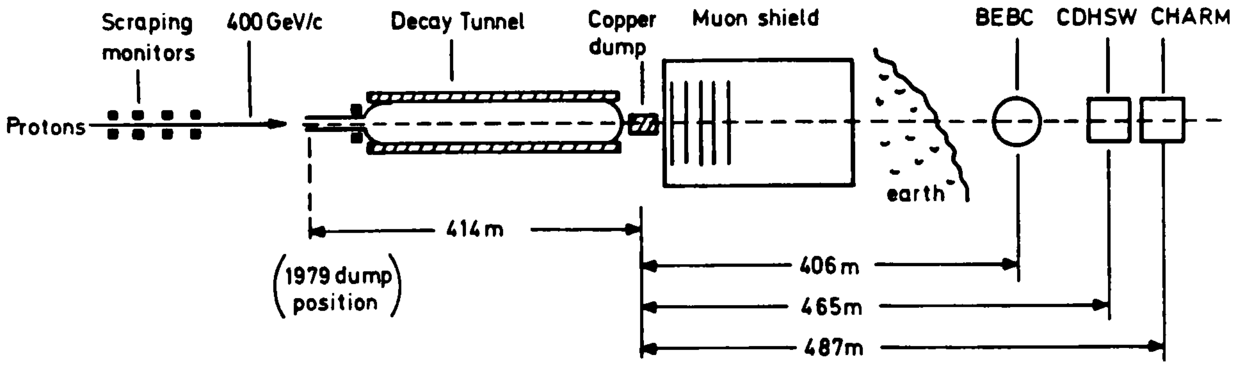

Figure 2.1 Experimental layout

installed at critical points in the line—i.e. after small apertures and steering points. These monitors are calibrated during the run by moving aluminium foils of known thicknesses ($7.1 - 71\,\mu$m) into the beam for a few spills, creating losses of the order of 10^{-5} to 10^{-3} at different positions.[1]

After the initial ejection and steering, the beam transport to the target consists of a 520 m section of straight vacuum pipe with no intermediate windows and no magnets. With a typical momentum spread of $\frac{\delta p}{p} = 1.5 \times 10^{-4}$, the beam spot at the target is still only 33 mm (4σ definition), half the width of the smallest aperture the protons pass through in the earlier steering. Beam-gas interactions are kept low by maintaining a pressure of less than 3×10^{-2} torr, and the gas composition is also checked. The distribution of matter in the beam is well known,[2] the only material in the beam being the vacuum end window (0.1 mm Ti) and a beam position monitor close to the dump, creating losses of around 18.7×10^{-4}. The conventional signal per proton is increased by a fraction 0.007 ± 0.001 and this is corrected for when the conventional and prompt signals are separated in chapter 4.

2.3 The Targets

At the centre of the experimental arrangement stands the dump itself. In this experiment three targets were used, a full density copper target and targets of fractional effective densities which are used in order to obtain the prompt neutrino rate by extrapolation. The full density target is a 3.025 m long block of solid copper. The one-half (one-third) density targets, also 3.025 m long, are arranged by using blocks with 2.5 (5.0) cm air gaps cut out after each 2.5 cm of copper (figure 2.2). The finite granularity of these targets has a negligible effect as the disc thicknesses and spacings are small compared with the hadronic interaction length (≈ 20 cm).

Behind the dumps, after an air gap of 2.5 cm, there is a 3.025 m long water-cooled copper catcher to absorb any hadrons emerging from the dump. The leakage of hadrons is significant for the one-third density dump, which has an effective length only just over 1 m of copper. Particles which emerge from the dump then interact in the full-density catcher, increasing the effective density of the whole system by a few percent. The appropriate

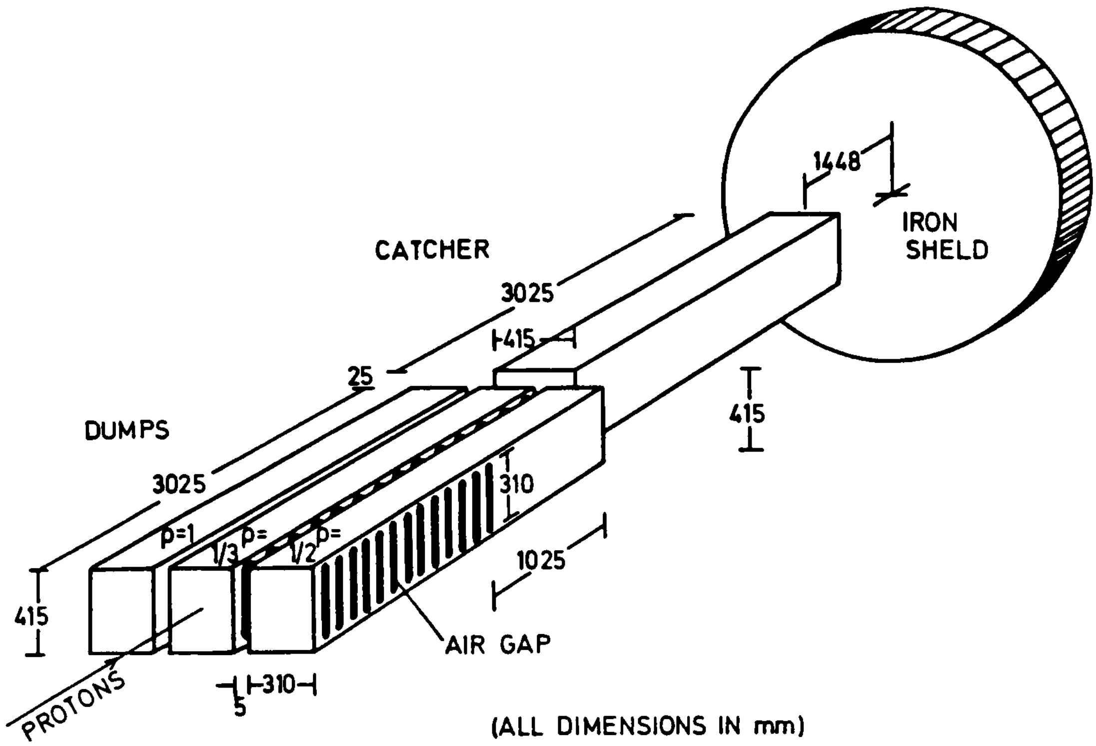

Figure 2.2 The Beam Dump Targets

correction is discussed in section 4.1. The cross-sectional are of the dumps, $31 \times 41.5\,\mathrm{cm}^2$, is more than adequate to contain the transverse development of the hadronic showers, preventing hadrons decaying to neutrinos in the air outside [3]. The power deposited into the dumps from the beam, which gives a shock audible above ground and outside all the shielding, is some 25 GW instantaneuously and 50 kW continuously. The required cooling created some technical problems during the run as the water pipe connections into the dump began to crack. The eventual solution was to change targets regularly, running for 16 h on full density and 8 h on one-third density each day.

2.4 The Shielding and Muon Gaps

The muons and neutrinos leaving the dump pass through a shielding system consisting of a 185 m section of steel followed by 173 m of local (mainly French) earth. Solid-state detectors measure the muon flux in five gaps in the steel whose distances correspond to minimum muon momenta of 14.7 − 175 GeV. The flux is measured radially in 15 cm intervals up to 45 cm from the beam axis. The detectors are calibrated absolutely by counting tracks in nuclear emulsion placed in front of the detectors and exposed for a few beam pulses. They are calibrated relative to one another during the run by moving a similar detector cyclically in front of the fixed detectors. The data from the muon gaps are used for three purposes; to constrain the neutrino flux calculations as these must also predict the flux of the muons, to check the linearity of particle flux in inverse target density and to calculate the correction for hadron leakage from the one-third density dump.

2.5 The Detectors

2.5.1 BEBC

A plan view of the detection system is shown in figure 2.3. Neutrino interactions are detected in the Big European Bubble Chamber [4]—BEBC—one of three detectors in the neutrino beamline. Although the bubble chamber is an order of magnitude less massive than the giant electronic detectors (CDHS and CHARM) it is an important counterpart as it is the only detector in which electron-neutrinos may be unambiguously identified and in which tau-neutrinos may be visually detected.

The boundaries of a volume inside the chamber (the fiducial volume shown in figure 2.4) are chosen avoiding the region close to the downstream wall, and excluding regions in which tracks are not sharply focussed by the fisheye lenses. This is done to ensure that tracks may be measured accurately and electrons may be identified. Situated 405.92 m from the rear of the target, BEBC fiducial volume subtends a total 46 μsr, ± 4.4 mrad horizontally and ± 3.1 mrad vertically. The chamber is filled with 75% molar Ne–H_2, a heavy liquid mixture being necessary to maximise the event rate. The density of the filling varied during the run between 0.685 and 0.750 tonne m^{-3} and the 16.9 m^3 fiducial volume contained a mean mass 11.5 tonnes, weighting the density for each run by the corresponding number of protons on target. The liquid is maintained at 29.3 K inside a magnetic field of 3.5 Tesla.

Bubbles formed by ionising particles in time with the beam-cycle are approximately 500 μ in diameter. The chamber is equipped with five cameras, four having standard fisheye lenses with a resolution of approximately 500 μ on axis and one which has a resolution of 200 μ on axis with a reduced angular acceptance and depth of focus. The lenses are arranged in a pentagon around the top of the chamber and the film is fed by a long transport mechanism to and from the camera backs which must be kept outside the magnetic field.

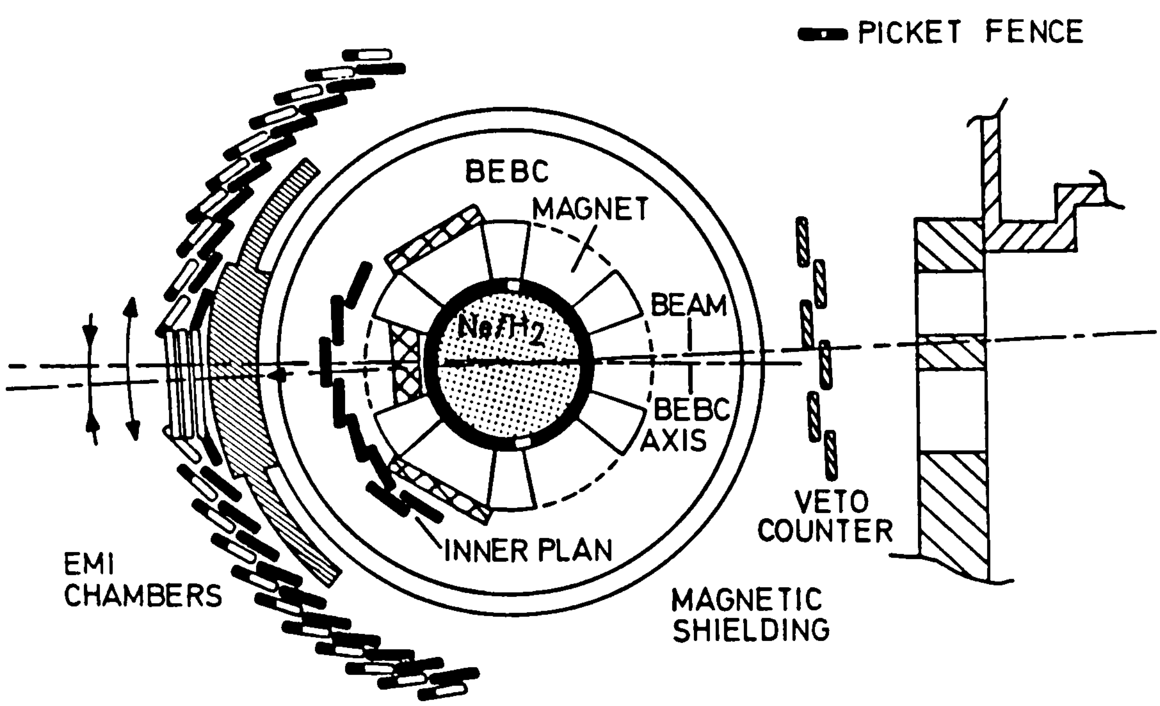

Figure 2.3 Plan view of the detection system

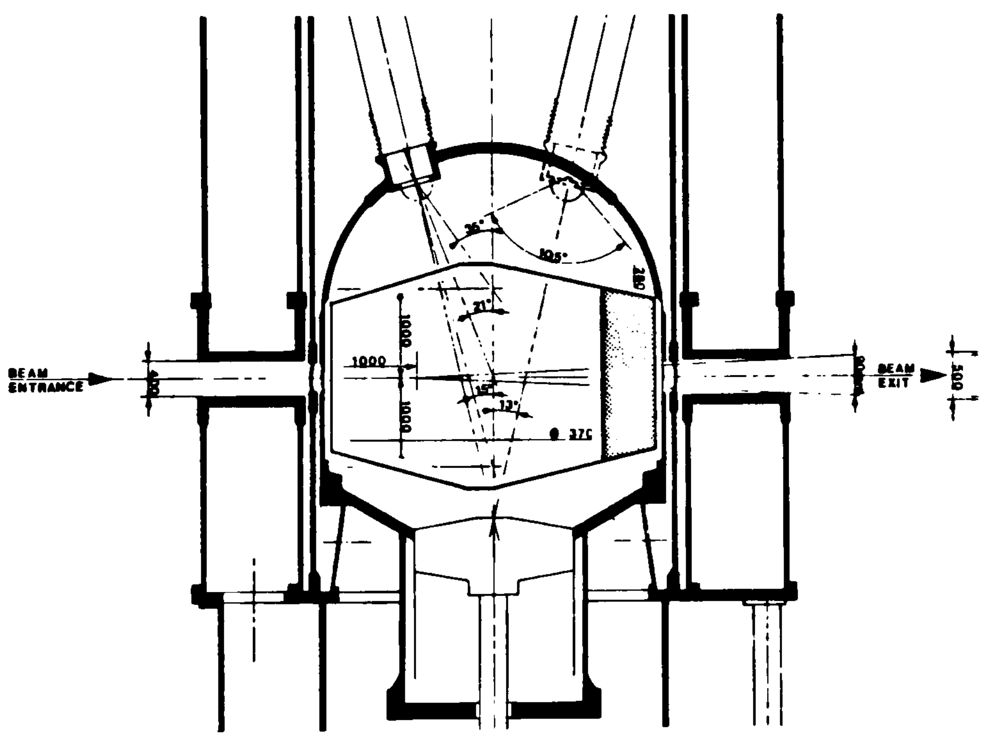

Figure 2.4 BEBC—Elevation and Fiducial Volume

2.5.2 The EMI

The bubble chamber is surrounded by electronic detectors designed to identify muons in the final states of neutrino interactions in an unbiased way and with high efficiency. The system was installed in two stages, firstly the External Muon Identifier (EMI) in 1977 and then the Internal Picket Fence (IPF) in 1981. The EMI [5,6] consists of two planes of multiwire proportional chambers, an inner plane of area $18\,m^2$, 4 m from the centre of BEBC and an outer plane of area $150\,m^2$ at 7.6 m. Between the planes, a layer of Iron up to 2.1 m thick is used as a hadron absorber. An additional plane of these detectors, $18\,m^2$ in area, is placed upstream of the bubble chamber to detect charged particles in showers entering the chamber. The efficiency of the EMI system is discussed in section 3.3.

2.5.3 The Internal Picket Fence

The IPF [7,8] is a proportional tube system mounted between the bubble chamber body and the vacuum tank wall. The IPF consists of 120 picket chambers each 10 cm wide and 2.2 m high arranged in a cylindrical ring at a radius of 2.0 m from the vertical axis of BEBC. In the measuring of events for this experiment, at least three leaving tracks were measured out to the wall wherever possible. The picket system is then able to associate the measured tracks with hits in the pickets. This gives a timing signal for all charged particles entering or leaving the bubble chamber.

This information is used to tidy up the information on events in several ways. The efficiency for muon detection is improved by the presence of a third plane of detector

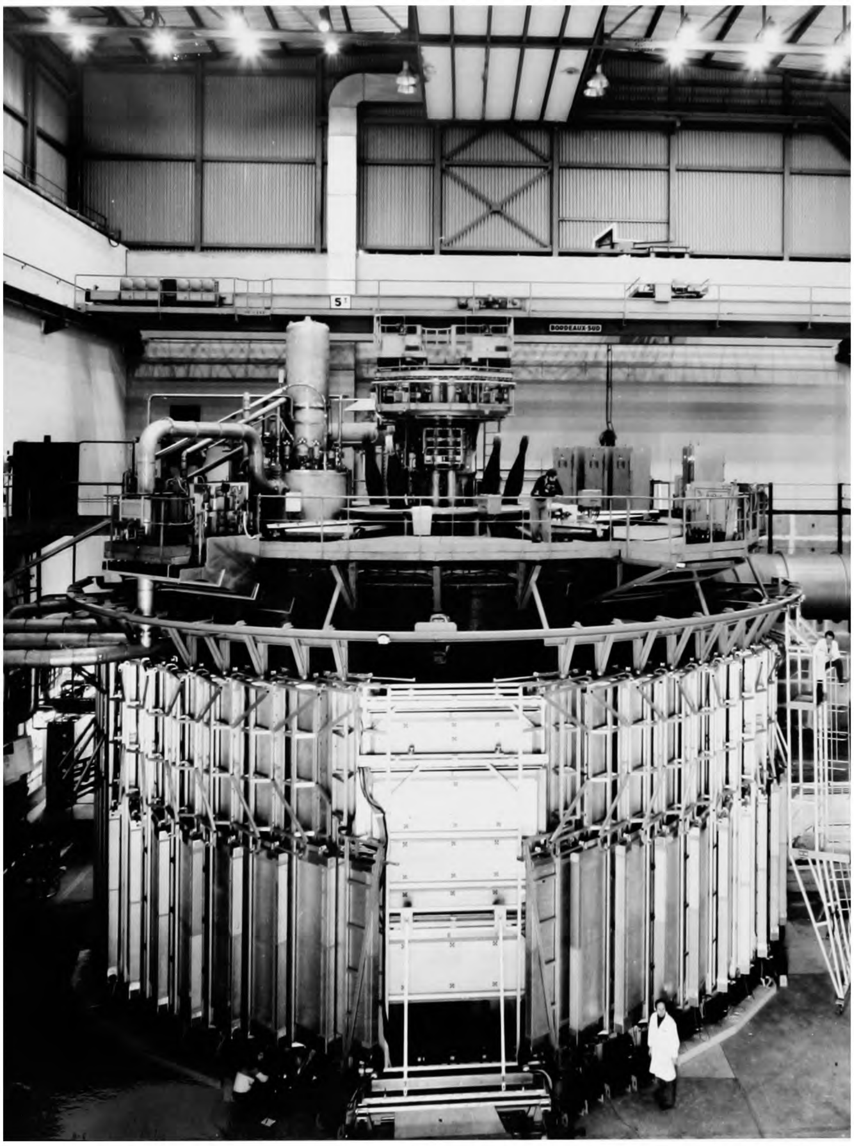

Figure 2.5 BEBC Hall and the EMI
(Reproduced by courtesy of PHOTO–CERN)

downstream, and the background of wrongly-associated muons (hadronic leaving tracks which extrapolate to a point on the EMI which has recorded a hit from a cosmic) is reduced because of the identification of the event timeslot. The upstream part of the picket fence can be used as an additional veto plane. It is also possible to use the IPF to decide whether two vertices on the same frame are associated, i.e. to distinguish re-interacting neutral tracks and independent neutrino events, again by the timeslot identification. The IPF has proved particularly useful together with the EMI as an off-line trigger for finding charged current events, and has been used to improve the efficiency for finding one-prong events (which are difficult to find on visual scans). The whole BEBC–EMI–IPF system was also used as a hybrid detector to measure the rate of neutrino interactions outside BEBC, to give an independent measurement of the prompt muon-neutrino rates (sections 3.6, 3.7).

2.6 Experimental procedure

The data taking started on February 20th and finished on September 13th 1982. Early on in the run, problems with the CERN power supply (which can be cut off at peak times in the winter) and with the dump cooling meant that the rate of protons on target was lower than hoped. In the later stages, the beam dump had high priority and by the end of the run some 3×10^{18} protons had been delivered to the dump and 260000 pictures had been recorded by each of the BEBC cameras. During the running a team of specialised technicians look after the bubble chamber. The film quality is checked by taking test strips at the beginning of and halfway through each roll (i.e. every 3000 pictures), so that problems with bubble density, flash timing etc. can be readily diagnosed. The EMI performance is also monitored continuously, with electronic scanning for voltage failures and manual checking for dead wires in the EMI chambers, using throughgoing cosmic muons in the 12 s between beam spills. Additional checks for possible systematic effects were made; the use of the half density target (see section 4.2.1), running with reversed field in BEBC and removing the beam catcher for a few beam pulses (section 4.1).

2.7 Scanning

Initially each BEBC frame was visually inspected in two independent scans and all candidate neutrino interactions were recorded and later measured. Hadronic interactions, signed by incoming tracks or by vertices in the walls, are also recorded and their frames are discarded. The event rate being low, the probability of a random coincidence of a neutrino event on a frame with a hadron event is very small. Discarded neutrino events can be corrected for later (section 3.2). Neutrino candidates were required to have a forward minimum-ionising track with a radius of curvature greater than 15 cm on any view or a pointing neutral conversion of effectively the same momentum. This corresponds roughly to requiring at least one track with a minimum momentum of 0.5 GeV. The interactions of electron-(anti)neutrinos were looked for during the normal scanning, then in the check-scanning performed by physicists, and lastly in a special check by a physicist of all the events with no EMI-identified muon. An event is classified as an electron-neutrino event if a single track from the primary vertex shows at least two of the following characteristic signatures :

(i) An e^+e^- pair pointing tangentially to the track—but not to the primary vertex.

(ii) An e^+e^- pair lying on the track and having at least 10% of the energy of the track itself.

(iii) A Delta-ray (knocked-on electron) taking at least 25% of the energy of the track.

(iv) A change of curvature without a visible kink.

Spirallisation inside the chamber was not considered a signature. Each candidate electron-neutrino interaction was inspected by a central group of physicists so that the sample could be treated as consistently as possible.

Before the events were measured, physicists at each laboratory were responsible for inspecting the events and checking that they had been scanned correctly. After the two initial visual scans, a further scan was done on a set of frames selected by an offline EMI–IPF trigger—frames with no veto and a track extrapolating through the IPF and EMI planes. The aim was to find all final state muons with a momentum greater than 3 GeV and to find an independent estimate of the visual scanning efficiency, which is considered in section 3.2. As a consistency check one roll was sent from each of the laboratories to be scanned elsewhere.

Further special scans were performed by physicists at some of the laboratories to look thoroughly at all the high resolution film (described in section 6.1.1), to look for tau-neutrino candidates in kinematically selected event samples (section 6.1.2)and to look for tau-neutrino candidates in the charged current events (section 6.1.3).

2.8 Measuring

After the scanning, the possible neutrino events found are measured on standard tables in order to get as complete a description of each track as possible. Each frame is measured on at least three views so that tracks and vertices can be reconstructed accurately in space. The film from the high resolution camera is not used for this purpose. All charged tracks from the primary vertex are measured, and secondaries from interactions are measured if the error on the incoming track is greater than 30%. Gamma conversions are measured if they occur within a distance of two radiation lengths of the primary interaction and neutral hadron vertices are always measured. The completed measurements are then run through a quality checking program, QUACK, so that badly measured tracks, duplicated tracks and other ambiguities can be sorted out, with a remeasurement if necessary. All frames are measured at least twice.

2.9 Data Processing

The data are then run through a geometry program which uses the point measurements and tables of optical and magnetic field data to evaluate the track momenta. The data from each laboratory were collected at CERN. As a consistency check, an independently produced file listing the frames, vertices, scan results and possible electron-neutrino frames accompanied the data from each laboratory, and discrepancies between this master list and the data on tape were sorted out. The information from the beam monitoring system, the EMI and the IPF is added frame by frame to the measurement data from the BEBC film and at this stage decisions about muon identification and re-interacting neutral association may be made. Primary electrons in electron-neutrino interactions are flagged by hand. The result is a data summary tape (DST) which contains complete frame by frame data for the experimental run. The DST represents the end of the purely experimental part of the work and the starting point for analysis.

References

[1] W.Kalbreier, CERN-SPS/ABT/TR/Note Tech/80–02 (1980).

[2] W.Kalbreier, CERN-SPS/ABT/TA/WK (1982).

[3] A.Grant, CERN-EF/0042M/ALG/ed (1980).

[4] G.Harigel (editor), *BEBC Users' Handbook* (CERN, 1977).

[5] C.Brand et al., *Nuclear Instruments and Methods* **136** (1976) 485.

[6] R.Beuselinck et al., *Nuclear Instruments and methods* **154** (1978) 445.

[7] H.Foeth, *Nuclear Instruments and Methods* **176** (1980) 203.

[8] C.Brand et al., *I.E.E.E. Transactions* NS29 (1982) 272.

3

Calculation of Event Rates

In this chapter the procedure for obtaining clean samples of neutral and charged current events is described. The raw event numbers are found and then corrected for experimental biases to give the best estimates of the true event rates corresponding to one-third and full density targets. A novel source of data has been used in this experiment—event rates are measured for the muons originating in neutrino interactions upstream of BEBC and passing through the IPF–EMI system. The ratio of neutral to charged currents is calculated for the whole sample and for the full-density sample of events, and we calculate the ratio for electron-neutrinos. The corrected rates from BEBC interactions and the throughgoing muon measurements are used in the next chapter to extract the prompt event rates.

3.1 Raw Event Numbers

The basis for the calculation of the prompt signal is the full data set on the DST described above in section 2.9. This contains experimental results in raw form, and in addition to well measured neutrino interactions there will be a number of cosmic ray interactions, some events with tracks which could not be accurately measured and events on frames which correspond to bad beam or detector conditions. To arrive at a clean sample of events, frames taken when there were hardware faults are excluded. Specifically, the beam control data must be complete and must indicate that the EMI–IPF system was up and working, the one-third or the full density target and the catcher were in position, no foils or monitors were in the beamline and the vacuum pressure must be less than 3×10^{-5} Torr. Beam losses are minimised by requiring that the last four scraping monitors read less than 150 mV per 10^{13} protons on target. It was found that making cuts on the other scraping monitors reduced the number of acceptable beam spills but did not change the rate of charged current interactions per proton on target. The corresponding number of protons on each target is summed over beam spills for which the same hardware conditions are satisfied and for which a good photograph was available on at least three views.

After this minimal filtering, the remaining events are looked at more closely. Neutral current interactions, for which the total event energy is unknown because of the missing final state neutrino, are treated differently and will be discussed in section 3.8. A good event is required to have its primary vertex—the point at which the interaction takes place—inside the fiducial volume of BEBC (section 2.5.1). Individual badly measured tracks (tracks which have at least 20% of the hadronic energy and an error $\frac{\delta P}{P} > 1$, or $E - P_l > 2\,\mathrm{GeV}$, or $P > 500\,\mathrm{GeV}$) are excluded. The primary electrons in events identified as electron-neutrino interactions and the EMI identified muons are flagged. If there are two primary leptons, the one with the largest momentum transverse to the neutrino beam direction is selected. In the absence of any new and unexpected effects, the second lepton comes from a charmed particle decay or from misidentifying a pion as a muon, and is included in the hadronic shower.

The last cuts made on the sample are kinematic; the events are required to have a certain minimum neutrino energy (to avoid cosmic-ray interactions and interacting neutral hadron tracks at low energy, coming from neutrino interactions in the material around BEBC), and the primary leptons are required to have momenta above 2.0 GeV (electrons) and 3.0 GeV (muons) above which their detection efficiencies are well known and can be corrected for, and the background of Dalitz pairs, Compton electrons and delta rays faking electron-neutrino interactions is small. To exclude cosmic ray interactions, events which have their total track momentum at a large angle to the beam direction (transverse component greater than 2 times the parallel component) or longitudinal component of momentum less than 0.3 GeV are also discarded.

The neutrino energy is the visible lepton energy plus 1.2 times the hadronic energy [1], the extra factor correcting on average for the loss of neutral particles in the hadronic shower—arrived at by scaling the hadronic momentum at constant direction until the event momentum transverse to the incoming beam is zero and averaging this scale factor over events. Final state baryon masses are excluded from the hadronic contribution to the neutrino energy estimate since these masses are present in the initial state target-nucleus. The raw event numbers are given with the corrected rates in table 3.1.

3.2 Corrections—Overall losses

3.2.1 Scanning losses

These numbers must now be corrected for losses of events and for misclassification of events between the neutral and charged current samples. Overall losses come from two sources—scanning losses and wrong associations with hadronic interactions. In this experiment there are two ways of estimating the scanning efficiency. The first method is to take all the events found on one of the independent scans (N_1 say) and to see how many of these were found on the other scan also (N_{12} say). The scanning efficiency for the second scan is the given by $e_2 = \frac{N_{12}}{N_1}$ and the combined scanning efficiency e is $e = 1 - (1 - e_1)(1 - e_2)$ resulting in an estimated efficiency of over 0.99 for all events with $E_\nu > 10\,\mathrm{GeV}$ in this experiment. The criticism of this method is that it must over-estimate the efficiency since it cannot take any account of the unknown number of events missed on both the scans. It is likely that there will be a set of undiscovered events with topologies different from most of the found events and for which the scan efficiency is therefore unknown. This method is only reasonably accurate if the number of missed events is known to be small.

The second method used was to perform a further independent scan of frames which were selected by a program which used the IPF–EMI data to predict frames likely to contain a charged current muon-neutrino interaction. The effectiveness of the prediction program itself is known, since we can see what fraction of the events already found are among its selected frames. After the scan (performed by a physicist in each laboratory concerned), the number of new events found is corrected for the effectiveness of the prediction program to give the likely true number of events not previously found, and this number as a fraction of all events found is the scanning loss. The results from this scan give efficiencies of 0.97 ± 0.02 (NC), $0.979 \pm .006$ (μ^-), 0.961 ± 0.015 (μ^+) and 0.99 ± 0.01 ($e^\pm$) for events with visible energy above 10 GeV. This result is less likely to be overoptimistic than that from the other method, and these values have been used to correct for the scanning losses.

3.2.2 Mis-association losses

Events are also lost by wrongly associating them with a hadron interaction upstream. In this experiment, because the low event rate reduces the chance of random associations, all frames containing interactions of incoming charged hadrons or containing vertices in the chamber wall itself are discarded. A good neutrino interaction may occasionally be lost on such a frame. The correction for this loss is made by finding the fraction of *all* frames lost in this way (recorded in scanning), this being the fraction of *good* events lost. The correction must be done separately for the full and one-third density samples. The result is that 0.99 ± 0.01 (0.978 ± 0.01) of good events are retained in the full (one-third) density samples.

3.3 Corrections—Misclassification of Muon Events

3.3.1 Introduction

Genuine charged current interactions will be included in the neutral current sample if the final state lepton is not identified. We must add the muons lost below the momentum cut, and correct the sample above the cut for the detection loss. Muons will not be identified by the IPF-EMI if they miss the outer EMI plane or if they miss both the picket fence and inner EMI plane ('geometrical' loss) or if they hit a faulty wire ('electronic' EMI loss.)

3.3.2 Muon momentum cut

The number of charged current events with muons below the momentum cut is calculated by summing over the energy distribution of the events seen above the cut and assuming a known distribution in the kinematic variable y, where

$$y = \frac{E_h}{E_\nu} = \frac{(1 - E_\mu)}{E_\nu}$$

The momentum cut truncates the range of allowed values for y, and the correction simply aims to calculate the loss event by event. The true number of events with a particular energy is proportional to the integral over the y-distribution between the limits $y = 0$ (hadron energy tends to zero) and $y = 1$ (muon energy tends to zero); the seen number of events has the limits $y = 0$ and $y = y_{max} = 1 - \frac{3}{E_\nu}$ (muon momentum tends to the cut-off). The seen events are therefore weighted by a factor

$$\frac{N_{true}}{N_{seen}} = \frac{\int_0^1 \frac{d\sigma}{dy}\, dy}{\int_0^{y_{max}} \frac{d\sigma}{dy}\, dy}$$

The y distribution used was obtained by integration over x of the (anti-)neutrino cross-section [2]

$$d^2\sigma \sim \frac{1+(1-y)^2}{2}F_2(x) + \frac{1-(1-y)^2}{2}xF_3(x)\ dx\,dy$$

giving

$$\frac{d\sigma}{dy} \sim \left(\frac{1+B}{2}\right) + \left(\frac{1-B}{2}\right)(1-y)^2$$

where

$$B = \frac{\int_0^1 xF_3(x)dx}{\int_0^1 F_2(x)dx}$$

The value $B = 0.8$ [2] is used for the corrections. For antineutrinos, the above formulæ are used with $B \rightarrow -B$.

3.3.3 Geometrical EMI correction

It is necessary to correct the number of muons seen by a factor which takes into account the geometrical acceptance of the IPF–EMI system. Whether a muon is inside or outside the acceptance depends on the position of the primary interaction inside BEBC and on the three components of the momentum of the muon produced. For the calculation of event rates, we are interested in the overall correction and can integrate over vertex positions in the fiducial volume and over muon production angles. It is necessary only to assume an energy spectrum for the events, which is assumed to be the observed spectrum. A monte-carlo program was used to find the acceptance loss, being the fraction of generated events in which the muon extrapolates outside BEBC without passing through the outer plane and at least one inner plane (IPF or EMI). The loss is 1.5% (0.7%) for μ^+ (μ^-) [3].

3.3.4 Electronic EMI efficiency

Muons are also lost if they pass a dead EMI wire or a faulty EMI chamber which fails to record a hit. Dead wires in the detectors are known from the continuous monitoring of the chambers. The fraction of faulty wires is not sufficient to give the inefficiency as the effect of a faulty wire depends on its position—i.e., on the expected flux of muons in the region affected. To estimate the loss of muons, a sample of kinematically selected muons was used; the selection requires a leaving track with its momentum transverse to the beam at a large angle with respect to the transverse momentum of the remaining particles. If such a track is found which extrapolates through a region of the EMI but which has not been identified as a muon because of a dead wire, the track is assumed to be a genuine muon. The electronic efficiency is 0.97 ± 0.02 [4].

3.4 Corrections—Misclassification of Electrons

Primary electrons from electron-neutrino interactions cannot be identified if the region near the primary vertex contains sufficiently many overlapping tracks that the electron cannot be followed reliably to the interaction vertex. The loss of electrons was estimated by comparison with a sample of events with final state muons. The muon sample was visually scanned to find the fraction of events on which the muon track could not be identified near the primary vertex. Assuming that the hadron shower behaves similarly in e and μ events, the loss from vertex confusion can be calculated. Further information was gained in a careful rescan of all the possible electron-neutrino candidates, and a comparison of the results gives the inefficiency. The overall loss of electrons in confused events is $5.3^{+4.9}_{-3.4}\,\%$ (e^-) and $2.7^{+1.8}_{-1.5}\,\%$ (e^+),[5,6] the charge dependence coming from the different hadronic energy spectra expected (y-distributions). Electrons are misidentified if they leave the chamber without giving the required minimum two signatures (as defined in section 2.7). This loss is greatest for interactions near the downstream boundary of the fiducial volume, although this boundary was chosen with electron detection in mind and the distance is approximately 1.3 radiation lengths (50 cm) at the centre. The loss was estimated by monte-carlo generation of signed electrons in BEBC,[5] and experimentally by using long electron tracks and considering what fraction of all possible vertex positions inside fiducial volume for that event would leave the required signatures within BEBC.[6] The estimated loss is $95 \pm 3\,\%$.

3.5 Corrected Event Rates—Results

After the corrections described, the rates are divided by the number of protons on each target—1.91 (0.81)$\times 10^{18}$ on full (one-third) density—and by the mass of the detector inside fiducial volume (11.5 t) to obtain rates corresponding to the same run conditions. The variation in the density of the BEBC filling is taken into account using an average weighted by the number of protons in good beam spills during each separate run. The corrected rates and the rates normalised to one tonne of detector and 10^{18} protons[7] are given in table 3.1.

Table 3.1 Corrected Event Rates

(Tp= Tonne of detector, 10^{18} protons on target)

$E_\nu > 10\,\mathrm{GeV}$		Raw	Corr	Corr/Tp
$\rho = \frac{1}{1}$	μ^-	344	412.5 ± 24.2	18.78 ± 1.10
	μ^+	108	121.7 ± 12.3	5.54 ± 0.56
	e^-	95	110.7 ± 12.1	5.04 ± 0.55
	e^+	27	29.9 ± 6.4	1.36 ± 0.29
$E_\nu > 10\,\mathrm{GeV}$		Raw	Corr	Corr/Tp
$\rho = \frac{1}{3}$	μ^-	410	495.5 ± 26.9	53.19 ± 2.89
	μ^+	134	153.1 ± 14.3	16.44 ± 1.53
	e^-	65	76.4 ± 9.9	8.20 ± 1.06
	e^+	24	27.0 ± 6.0	2.90 ± 0.64
$E_\nu > 20\,\mathrm{GeV}$		Raw	Corr	Corr/Tp
$\rho = \frac{1}{1}$	μ^-	282	325.1 ± 20.6	14.80 ± 0.94
	μ^+	81	90.1 ± 10.3	4.10 ± 0.47
	e^-	91	105.4 ± 11.9	4.80 ± 0.54
	e^+	22	23.9 ± 5.7	1.09 ± 0.26
$E_\nu > 20\,\mathrm{GeV}$		Raw	Corr	Corr/Tp
$\rho = \frac{1}{3}$	μ^-	331	384.8 ± 22.7	41.31 ± 2.44
	μ^+	100	113.1 ± 11.8	12.14 ± 1.27
	e^-	59	68.7 ± 9.2	7.37 ± 0.99
	e^+	20	22.3 ± 5.4	2.39 ± 0.58

3.6 'Near' Throughgoing Muons

3.6.1 Introduction

We will see in the next chapter that the prompt rates for $\mu^{\pm}$ events in BEBC have large errors and are not significantly different from zero. To increase statistics the BEBC–IPF–EMI system was used as a hybrid detector. The 'target' in this set-up is the region between the veto plane of the EMI and the upstream picket fence. The magnet coils which generate the BEBC field and the iron flux shielding contribute altogether 55.2 ± 2.8 Tonnes—around five times the mass of the fiducial volume inside BEBC. The trigger for a charged current muon-neutrino interaction is a 'four-fold coincidence', i.e. hits in both picket fence planes and both EMI planes. It is also required that the muon extrapolates to a point on the veto plane and that there is no hit in the veto region within the error ellipse of the extrapolation. This ensures that the muon comes from the target region expected and not from interactions in the shielding further upstream. The z (height) and dip distribution for the muons shows that they are well correlated with the neutrino beam direction.[8]

3.6.2 'Near' throughgoing muons—experimental procedure

Four-fold coincidences were found using the IPF–EMI data, and by fitting tracks through the four hits in the chambers the positions of the entry and exit points of the muon tracks in the BEBC wall were predicted. A list of frames expected to contain muons traversing BEBC (throughgoing muons) was circulated to the participating laboratories so that the frames could be measured. This enabled the tracks to be found easily, and the use of automatic measuring meant that the whole procedure could be done quickly—single muons with an entry point fixed in the wall are easy for these machines to track. This meant that the data was ready to supplement the BEBC data during the analysis stage. The measured momenta are combined frame by frame with the electronic data to extrapolate the track accurately to the veto plane, so that the origin of each muon is established. The data set for analysis is then the sample of measured muons which reliably originate in our target region.

3.6.3 Throughgoing muons—Results

The numbers of seen interactions are corrected for the electronic and geometrical efficiencies. The correction factors which must be included are the electronic efficiencies of the four planes (the probability that a muon passing through the planes triggers each plane), the geometrical acceptance of the 4–plane system (the probability that a muon originating in the target region will pass through the four planes) and the probability that the veto plane is noise free (i.e. that the muon is not vetoed by extrapolation to a point on the plane which has been hit by a cosmic or a track from an unassociated upstream interaction). The electronic efficiencies were estimated from the EMI information detailing dead wires etc. The geometrical acceptance was found [9] by generating neutrino events in the target region with the spectrum observed in BEBC, and by generating the muon momenta according to the Buras and Gaemers parametrization of the structure functions [10]. The generated muons are tracked through space to see what fraction pass through the four planes. Reasonable variation of the neutrino spectrum in angle and energy does not change the results within errors. The corrected number of events is the BEBC equivalent number per tonne and 10^{18} protons, noting that the effective number of protons is different for the throughgoing muons. The results [9] are given in table 3.2.

Table 3.2 'Near' Throughgoing Muon Rates

	$\rho = \frac{1}{1}$		$\rho = \frac{1}{3}$	
$E_\nu > 10$	Raw	Corr/Tp	Raw	Corr/Tp
μ^-	590	18.5 ± 1.5	590	50.4 ± 4.0
μ^+	189	4.8 ± 0.5	154	10.5 ± 1.1
$E_\nu > 20$	Raw	Corr/Tp	Raw	Corr/Tp
μ^-	405	14.7 ± 1.2	394	38.4 ± 3.3
μ^+	131	3.6 ± 0.4	92	6.8 ± 0.9

3.7 'Far' Throughgoing Muons

The final source of data on the muon-neutrino rates is the flux of muons reaching the IPF–EMI planes from interactions outside the detection system altogether. The muons are signed by coincident hits in all five detector planes. Their z and dip distributions are centered round the beam axis and the charge ratio $N(\mu^+) : N(\mu^-) = 0.35 \pm 0.01$ rules out an origin from pion, kaon or vector meson decays [11]. Muon momenta were reconstructed by fitting tracks through the five hits, and this procedure was checked by measuring the throughgoing muons on two BEBC rolls. The measured tracks and the constructed tracks give consistent results with the mean ratio of the measured to constructed momentum being 0.99 ± 0.09 [11].

The acceptance for these muons, most of which originate in the earth some $50 - 150\,\mathrm{m}$ from BEBC, [12] has been calculated [13] so that the rates may be compared with the BEBC results. The method is essentially the same as for the near throughgoing muons, but the matter distribution upstream has to be included in the model so that the scattering and energy loss processes may be taken into account. The absolute normalisaton of the rates has a large uncertainty which cancels when taking the ratio of prompt to full density rates; the results appear in the next chapter.

3.8 Neutral Current Events

3.8.1 Introduction

The ratio of neutral to charged current interactions (NC:CC) in this experiment is a very useful quantity. Since we have a sample of high energy electron-neutrino interactions which is a significant fraction of the total, we are able to calculate the ratio NC:CC for electron-neutrinos alone. The experimental NC:CC ratio is also used in chapter 7 to place an upper limit on the fraction of the prompt signal which can be attributed to interactions of the tau-neutrino. So far, event rates have only been calculated for the charged currents. The neutral currents are not directly comparable as the neutrino in the final state means that the event energy is unknown. In a comparison of neutral and charged current events it is necessary to use the hadronic part of the event energy as the basis for comparison. The other major difference is that the events which have a genuine charged lepton in the final state are all neutrino interactions, whereas the events with no visible charged lepton will be a mixture of hadronic background and neutrino interactions (after misidentifications have been corrected for).

3.8.2 The hadronic background

Two methods have been used to separate the hadrons from the genuine NC events. The first uses the difference in event energy and energy balance. An incoming hadron carries only a fraction of the event energy outside BEBC in which it was produced, and the contamination is expected to be significant only at low energies. The neutrino events will be distinguished by having significant missing momentum transverse to the beam direction whereas the hadronic events should be well balanced. The other method [14] uses the different spatial distribution of events inside BEBC, the neutrinos interacting uniformly in space and the hadrons interacting with a typical path length of around half the BEBC diameter. It is necessary to take into account the path length in the chamber which is available for a particle traversing the chamber to interact in (the potential length); this has been done directly by dividing the neutral rate in a given x–coordinate bin by the charged current rate (which should have a flat distribution in space.) This ratio is fitted as the sum of a constant term and an exponentially falling term. The constant term gives the required NC:CC ratio and the relative sizes of the terms will give the ratio of neutrinos to hadrons. This method stretches the statistics available here somewhat, but it has the advantage of removing the hadronic contamination in a direct manner. It is a comfort to note that the two methods agree well (see below).

3.8.3 Correcting the neutral and charged current event rates

Cuts in hadronic energy and transverse momentum are used here to obtain a comparison of neutral and charged current events. This is done so that we may compare our results with those obtained in an earlier BEBC experiment (WA47) [15] with minimal systematic errors, as the same method was used. The treatment of the data is very similar to that described for the charged currents, but care has to be taken over the corrections. The mis-identification losses in the charged current sample correspond to events which have been wrongly assigned as neutrals because the final state lepton was not seen. It should be

Table 3.3 Neutral and Charged Current Rates

$E_h > 10\,\mathrm{GeV}$, $\rho = \frac{1}{1}$		Raw	Corr	Corr/Tp
$P_h^T > 1\,\mathrm{GeV}$	μ^-	185	209.20 ± 15.57	9.47 ± 0.71
	μ^+	34	37.97 ± 6.55	1.72 ± 0.30
	e^-	51	58.25 ± 8.52	2.64 ± 0.39
	e^+	12	13.74 ± 3.99	0.62 ± 0.18
	NC	112	96.45 ± 10.24	4.37 ± 0.46

$E_h > 10\,\mathrm{GeV}$, $\rho = \frac{1}{3}$		Raw	Corr	Corr/Tp
$P_h^T > 1\,\mathrm{GeV}$	μ^-	195	224.35 ± 16.28	24.26 ± 1.76
	μ^+	49	55.51 ± 7.99	6.00 ± 0.86
	e^-	37	42.84 ± 7.27	4.63 ± 0.79
	e^+	9	10.40 ± 3.48	1.12 ± 0.38
	NC	129	115.48 ± 11.39	12.49 ± 1.23

noted that the estimated event energy is different for the misidentified event; a lepton which finds its way into the hadron shower will have its energy scaled up by the factor 1.2 which accounts for lost neutrals. Events which have hadronic energies below the cut therefore contribute to the neutral current events above the cut, and must be retained when making the corrections. Similarly, the hadronic transverse momentum will change when the lepton is included in the hadron shower. The correction for the minimum lepton energy cut assumes *all* leptons below that cut are in the neutral sample; leptons *correctly identified* but below the cut must be mis-assigned deliberately. Applying these cuts and correcting the events for overall losses, the rates given in table 3.3 are obtained.

3.8.4 The neutral to charged current ratio

We find that the ratio of neutral to charged currents for events which satisfy these cuts is 0.332 ± 0.027 for the whole data sample and 0.302 ± 0.037 for the full density sample. The corresponding results from the fit to the spatial distributions are [16] 0.355 ± 0.042 and 0.32 ± 0.06, in agreement.

3.9 The Neutral To Charged Current Ratio For Electron-Neutrinos

Assuming lepton universality it is expected that the neutral to charged current ratio for electron-neutrinos (R_e) should be equal to that for muon-neutrinos (R_μ). The ratio for electron-neutrinos alone cannot be measured in conventional neutrino experiments at high energy as the muon-neutrino flux dominates. The analysis of counter-detector results from the beam dump also requires a value of R_e to calculate the charged current electron rate. The neutral currents expected from the observed $\mu^{\pm}$ rate are subtracted from the total neutral currents and it is assumed that the remaining neutral currents are associated with $(R_e)^{-1}$ charged current electron-neutrino interactions.

It is therefore of both theoretical and experimental interest to attempt to measure R_e, which we're able to do as we have a large number of electron-neutrino interactions (a fraction ≈ 0.2 of the CC sample). We assume that the contribution to the events from tau-neutrino interactions may be neglected. Then

$$R_e = \frac{\text{NC} - N_{\mu^+} R_{\mu^+} - N_{\mu^-} R_{\mu^-}}{N_{e^+} + N_{e^-}}$$

We use the values $R_{\mu^-} = 0.345 \pm 0.015$ and $R_{\mu^+} = 0.364 \pm 0.029$ from WA47, and neglect systematic errors.

The value for electron-neutrinos (obtained for the $\nu_e - \bar{\nu}_e$ mixture in this experiment) is $R_e = 0.23 \pm 0.16$. This is clearly consistent with universality, the large error unfortunately being inevitable because the electrons are a fraction of the charged current sample (or equivalently because of the subtraction of the large muon-neutrino contribution to the neutral currents). The result is very sensitive to the input data. Had we used an NC:CC ratio from the spatial fit and R_μ values from a different experiment we would have found $R_e = 0.47 \pm 0.20 \pm 0.15$ [17]. If the electron-neutrino coupled to the tau lepton we would expect a value $R_e \approx 0.6$ [17], and we cannot rule this out at a high confidence level.

References

[1] H.Deden et al, *Nuclear Physics* **B149** (1979) 1.

[2] F.E.Close, *An Introduction To Quarks And Partons* (Academic Press, 1979) 245-7.

[3] H.Kreutzmann, WA66 note.

[4] H.Klein, P.Schmid, H.Wachsmuth, WA66 notes.

[5] Bonn Group, WA66 notes.

[6] J.Guy, WA66 note.

[7] WA66 Collaboration, paper in preparation.

[8] H.Wachsmuth, WA66 note.

[9] H.Kreutzmann, WA66 note.

[10] A.J.Buras and K.J.P.Gaemers, *Nuclear Physics* **B132** (1978) 249.

[11] H.Wachsmuth, W.Venus WA66 note.

[12] L.Pape, WA66 note.

[13] W.Venus, WA66 note.

[14] A.Vayaki, K.Hultqvist, J.Krstić, WA66 notes.

[15] P.C.Bosetti et al., *Nuclear Physics* **B217** (1983) 1.

[16] J.Krstić WA66 note.

[17] P–O. Hulth, WA66 note.

4

The Prompt Rate and its Interpretation

The rates tabulated in the previous chapter are used to extract the prompt part of the signal—by extrapolation to infinite target density and by subtraction of the conventional rate. Assuming that the prompt rate may be attributed to hadronic charm production and semileptonic decay in the dump, the possible charm production mechanisms and their corresponding cross-sections are discussed.

4.1 Catcher Correction

Before we can extract prompt rates from comparison of the full and one-third target density data, we must take account of the effect of pions and kaons emerging from the one-third density dump and interacting or decaying in the full density catcher. Effectively this can be regarded as a change in effective density, or equivalently as an adjustment of the conventional flux component from the one-third density arrangement. The experimental method used to measure the leakage of pions and kaons from the target is discussed and the appropriate value of the effective density is calculated.[1]

A short section of the experimental run was dedicated to the measurement of the hadron flux emerging from the fractional density dumps. The catcher was moved in and out of its position behind the dump for each of the three targets in turn—about 50 proton beam pulses were recorded for each separate arrangement. The change in the measured muon fluxes in the shielding gaps are attributable to two effects:

(1) The muon rate increases by a factor f_{ms} in all the catcher out configurations compared with catcher-in. This is because the muons are multiply scattered by less material, and they pass into the shielding with roughly 5 GeV more momentum.

(2) For the one-third density target, there is an additional flux increase because the leaking pions and kaons now have a path of around 3 m in air in which to decay.

Referring to figure 4.1, we see that the average distance travelled by a particle after the dump is $L + \lambda_{\rm Fe}$ (for the catcher-out configuration) and $\epsilon + \lambda_{\rm Cu}$ (catcher-in). The ratio of these lengths, k, gives the sensitivity of the catcher-out arrangement for the measurement of leakage from the catcher-in arrangement. Suppose a rate R_1 is observed for full density catcher-in, and a rate R_3^{obs} is observed for one-third density catcher-in. We write $R_3^{obs} = R_3 + C_L$, R_3 being the rate from the physical dump and C_L being attributed to decays after the dump. For one third density, the rates catcher-out and catcher in will have a ratio

$$r = \frac{R_3 + kC_L}{R_3 + C_L} f_{ms}$$

dividing this by the same ratio for full density will remove the multiple scattering factor, since the leakage from full density will be zero. The remaining factor r_3 is the rate we are interested in for measuring the leakage correction, and

$$r_3 = \frac{R_3 + kC_L}{R_3 + C_L} = 1 + \frac{(k-1)C_L}{R_3^{obs}}$$

From this expression, C_L is the unknown which can then be calculated. The additional flux coming from an ideal one-third density dump, originating in the region after the real dump ends, is given by the leakage rate C_L weighted by the decay length ratio for the two arrangements, (see figure 4.1)

$$\begin{aligned} R_3^{ideal} &= R_3 + C_L \left(\frac{3\lambda_{\text{Cu}}}{\lambda_{\text{Cu}} + \epsilon} \right) \\ &= R_3^{obs} + C_L \left(\frac{3\lambda_{\text{Cu}}}{\lambda_{\text{Cu}} + \epsilon} - 1 \right) \end{aligned}$$

The correction should be obtained for each muon gap independently as the extra flux will be energy dependent. For correcting overall numbers of neutrinos with energies above a given cut, a single parameter will suffice, and the choice here will be to express this as a change in effective density of the target, from $\frac{1}{\rho} = 3$ to $\frac{1}{\rho} = 2.92 \pm 0.02$.

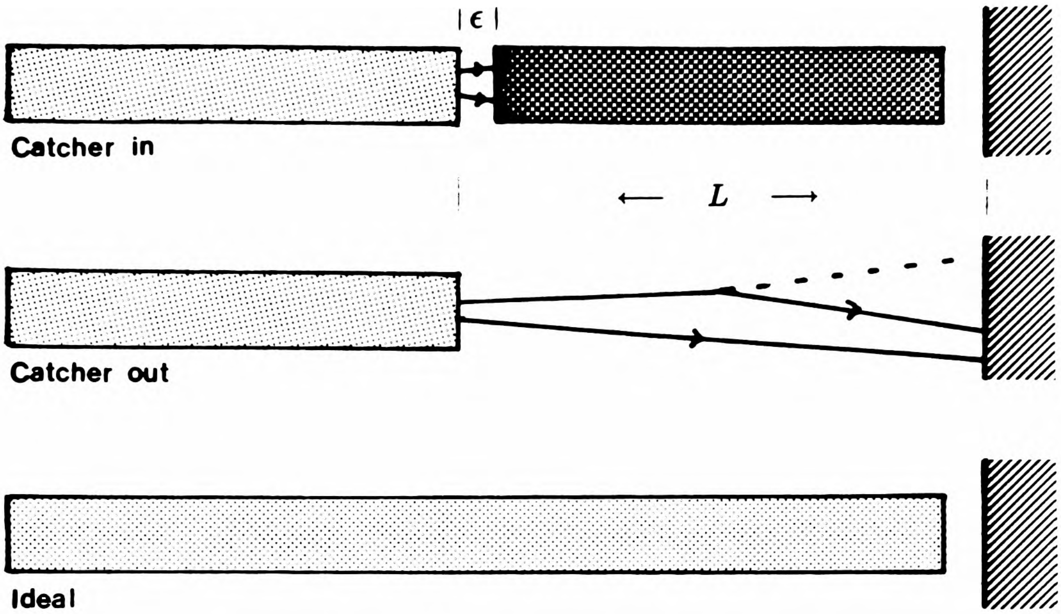

Figure 4.1 One third density arrangements
Light shading for one-third density, heavy for full.
Shielding is shaded diagonally

4.2 Extrapolation Method for the Prompt Rates

4.2.1 Linearity of the signal

With corrected rates on both the full and one-third density targets we can proceed to calculate the prompt and conventional components by extrapolation to infinite dump density. The justification for this procedure is that the number of pions and kaons which decay is inversely proportional to target density, and the conventional signal must vanish in this limit. To check the linearity of the signal with inverse dump density, the half density target was used for a few beam spills. The solid state muon detectors in the muon gaps should record a non-prompt signal which is linear in $\frac{1}{\rho}$. In fact a departure of $1.0 - 2.5$ % (gaps 2–4) was noticed, the rate on half density being below that expected from the other targets. The disc spacings in the fractional density targets were then measured and the half-density target was found to have an effective $\frac{1}{\rho}$ of 0.503 [2]. The one-third density target was accurate within the errors. In addition it was estimated that the half density target runs 100°C cooler than the others as it is not in the beam long enough to heat up. Evidence for the expansion of the other dumps is an increase in muon rate over the first section of each run. When these effects are taken into account, [2] the fluxes are linear within the measuring error of 0.5%. Note that we have measured the coefficient of linear expansion of copper.

4.2.2 Results

To calculate the prompt component of the neutrino event rate by extrapolation we write the expected rates R_1 and R_3 on the full and one-third density arrangements as a sum of a conventional part and a prompt part. The fraction of conventional neutrino flux on full density target which is expected to come from interactions of the beam protons upstream of the dump $\beta = 0.007 \pm 0.001$ and the effective inverse density of the one-third density arrangement, $\frac{1}{\rho} = 2.92 \pm 0.02$. The prompt rate is then the solution of the simultaneous equations

$$R_1 = P + C(1 + \beta)$$

$$R_3 = P + C\left(\frac{1}{\rho} + \beta\right)$$

and the prompt rate P is

$$P = \frac{(\frac{1}{\rho} + \beta)R_1 - (1+\beta)R_3}{(\frac{1}{\rho} - 1)}$$

which reduces to the correct form $P = \dfrac{3R_1 - R_3}{2}$ for an ideal ($\beta = 0, \frac{1}{\rho} = 3$) arrangement. The prompt event rates are presented in table 4.1.

The rates shown for near muons are acceptance corrected rates and can be compared with the BEBC rates. The figures for far muons are the acceptance corrected values for the ratio of prompt to full density rates (0.152 ± 0.023 for μ^-, 0.340 ± 0.040 for μ^+) multiplied by the full density muon rates actually measured in BEBC. The far muons establish a prompt signal in both channels. The results are not strictly comparable with the BEBC rates as the cut made to ensure that magnetic field effects near the bubble chamber could be neglected ($p_\mu > 20\,GeV$) means that the figures are insensitive to the neutrinos below $30 - 40\,GeV$ energy.

4.3 Subtraction Method for the Prompt Rates

4.3.1 Introduction

The subtraction method requires a model for the calculation of the conventional rate which can be tuned by fitting the muon flux data. The calculation [3] begins with the sources of conventional neutrino fluxes. Decaying pions and kaons yield muon-neutrinos and the semileptonic decays of kaons, lambdas and sigmas all contribute to the electron-neutrino flux. To calculate the flux, we require a model for the production of these particles

Table 4.1 Prompt Rate By Extrapolation

events/Tp

(a) BEBC Data

E_ν	μ^-	μ^+	e^-	e^+
> 10	0.73 ± 2.08	-0.18 ± 1.11	3.38 ± 0.97	0.54 ± 0.53
> 20	0.89 ± 1.80	-0.12 ± 0.94	3.46 ± 0.93	0.40 ± 0.48

(b) Throughgoing muons

E_ν	Near μ^-	Near μ^+	Far $\mu -$ *	Far μ^+ *
> 10	3.0 ± 3.0	2.0 ± 0.9	—	—
> 20	2.9 ± 2.5	2.0 ± 0.7	2.25 ± 0.37	1.39 ± 0.23

* See text.

in the beam dump target. This model will of course predict both the muon and the muon-neutrino fluxes coming from the decays. The measurement of the muon flux in the shielding gaps can be used to constrain this calculation and the implied neutrino flux accompanying the muons can be determined absolutely.

4.3.2 Muon flux measurements

Muons are measured at five points in the iron shielding following the dump. These muons lose energy as they traverse the iron, and measuring the fluxes in these different locations enables a fit to be made to the muon spectrum. The detector in gap 1 is not used in this experiment as it is very near the dump and is saturated for most beam spills. In a typical pulse of 10^{13} protons delivered to the target, the detectors measure of the order of $10^3\,\mathrm{muons\,cm^{-2}}$. The numbers are corrected for multiple scattering losses. The charge of the muons is not determined. The rate in each gap is measured for full one-half and one-third target densities, and is found to be linear in inverse density within measuring errors. The extrapolation to zero inverse density enables the non-conventional muon signal to be extracted— this does not correspond to the 'prompt' signal in the usual sense as it contains muons which are not associated with neutrinos but which come from electromagnetic decays of mesons eg. $\phi \to \mu^+\mu^-$ or from the Drell–Yan process. The resulting conventional flux is then fitted to the production model.

4.3.3 The flux calculation model

We do not know the proportions of μ^- and μ^+ from the measured flux, nor what fraction of the spectrum at any given energy comes from π or K decay. In order to calculate the type (ν or $\bar{\nu}$) and energy of the accompanying neutrinos, we need a model with the appropriate $\pi^{\pm}$ and $K^{\pm}$ ratios as a function of energy. Previous experiments have relied on particle production spectra measured on Be targets with incident 400 GeV protons and used data taken on several targets at 24 GeV momentum (scaled up to 400 GeV) to convert these spectra to those expected from copper. Before this experiment, measurements were made of production spectra for 400 GeV protons on copper targets of different thicknesses, allowing the energy spectrum of each secondary to be determined for the beam dump taking into account thick target effects. The absolute normalisation of the data was uncertain because of unknown systematic errors arising from secondary beam problems, and was left as an adjustable parameter in the fit to the muon fluxes. This fit of the model to the measured fluxes gives the conventional muon flux shown in table 4.2. The electron-neutrino flux is dominated by the K°, $\overline{\mathrm{K}}^{\circ}$ contributions.

4.3.4 Subtraction method—result

It is now a simple matter to subtract the conventional rate from the corrected data to obtain the prompt signal. The one-third density data can also be used, where $\frac{1}{\rho}$ times the conventional flux shown is subtracted, and should give the same prompt flux within errors. The best estimate of the prompt signal by subtraction is the weighted mean for the two different target densities.

4.4 Summary

4.4.1 Comments on the prompt rates

Prompt rates have been established for $e^{\pm}$ and $\mu^{\pm}$ events. The fitting of the above data are presented and discussed in the WA66 paper [4] and the results are reproduced here for completeness. Fitting the BEBC extrapolated and subtracted rates and the near thoughgoing muon rates gives the ratio for $E_{\nu} > 20\,\mathrm{GeV}$

$$\frac{N_{e^+} + N_{e^-}}{N_{\mu^+} + N_{\mu^-}} = 2.12 \pm {}^{1.68}_{0.68}$$

and the asymmetry, which is a preferable quantity as the denominator is not compatible with zero,

$$A = \frac{N_{e^\pm} - N_{\mu^\pm}}{N_{e^\pm} + N_{\mu^\pm}} = 0.36 \pm {}^{0.22}_{0.18}$$

The prompt e^+ to e^- event ratio, 0.21 ± 0.06 is significantly below the cross-section ratio 0.47 [5]. Work on the far muons in the lower energy range is still in progress.

Table 4.2a The Conventional Signal
(full density target)

events/Tp

E_ν	μ^-	μ^+	e^-	e^+
> 10	19.52 ± 1.56	4.99 ± 0.04	1.07 ± 0.13	0.46 ± 0.06
> 20	14.65 ± 1.17	3.11 ± 0.77	0.77 ± 0.92	0.33 ± 0.04

Table 4.2b Prompt Rates by Subtraction

E_ν	μ^-	μ^+	e^-	e^+
> 10	-1.79 ± 2.70	0.91 ± 0.90	4.30 ± 0.57	1.09 ± 0.30
> 20	-0.43 ± 2.10	1.59 ± 0.66	4.36 ± 0.52	0.96 ± 0.26

4.4.2 Comparisons with other experiments [6]

The results of the CERN experiments have been compared at the summer conferences and a brief summary is presented here.

(i) Compared with the previous BEBC beam dump experiment, our present event rates are low. The geometrical acceptance of BEBC has been increased by a factor ≈ 4.2 and the event rates are expected to increase by a factor 3.3–3.5 allowing for the angular dependence of the flux. The actual ratio for μ^- is lower than this (≈ 2.9) but compatible within 2σ [7].

(ii) The electron-neutrino event rates measured by the three CERN experiments are compatible. The muon rates obtained by CDHS agree with the BEBC rates and CHARM report a higher rate, and consequently a lower ratio of prompt electrons to muons.

(iii) The asymmetry parameters measured by BEBC and CDHS are consistent with zero. CHARM find an excess muon signal at $\approx 4\sigma$.

(iv) The μ^+ to μ^- ratio measured by CDHS is 0.34 ± 0.11 which is consistent with equal fluxes and also with the BEBC result.

The conclusion is that we should approach the estimation of the cross-section for charm production with caution !

4.5 Charm Production

4.5.1 Assumptions and models

The prompt neutrino rate is interpreted as evidence for the production and semi-leptonic decay of charmed particles in the beam dump target. The reasoning which leads to this conclusion in discussed in the papers presenting the first beam dump results (chapter 1 refs. [1–3]). The charm production cross-section necessary to account for our prompt event rates can be calculated provided that we make assumptions to allow for the following:

(i) The spectrum of protons in the target allowing for cascading effects. The model is described in section 5 and the spectrum is plotted in figure 5.1.

(ii) The s-dependence of the charm production cross-section (so that the contribution of the low energy protons in the cascade can be calculated relative to that from the 400 GeV primaries.) Here we assume a cross-section proportional to $s^{1.3}$.

(iii) The charmed particles produced—we require the mixture of Λ_c^+, D^+ and D° which is responsible for the ν_e flux and similarly the proportions of D^- and $\overline{D}^\circ$ for $\bar{\nu}_e$. This must be calculated by fitting spectra for different parent particles.

(iv) The differential production cross-section, which we parametrize as

$$E\,\frac{d^2\sigma}{dx_F\,dp_T^2} \sim (1-\mid x_F \mid)^n\; e^{-bp_T}$$

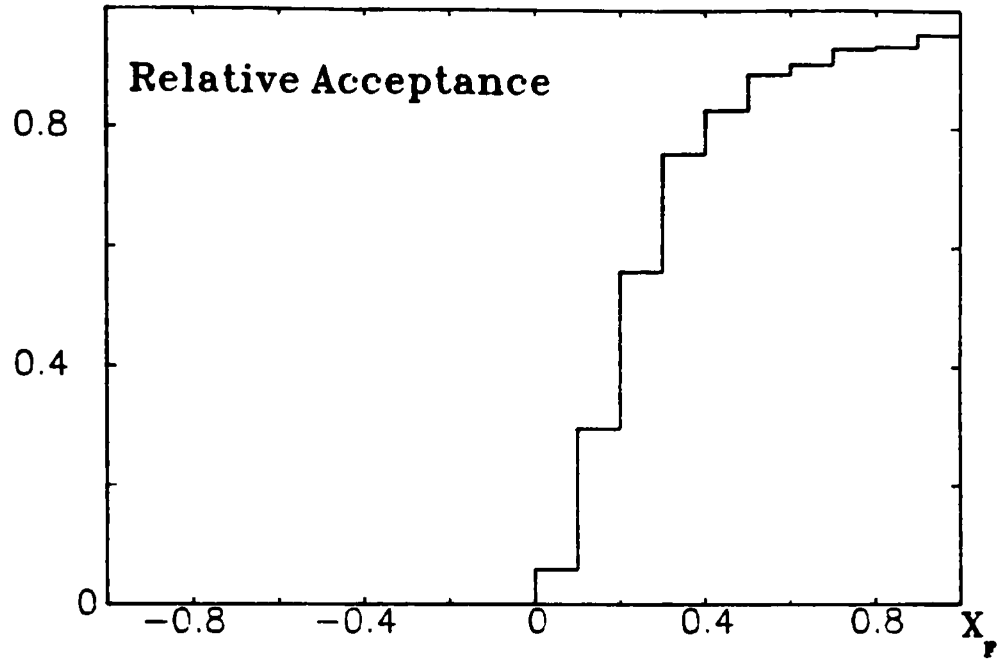

Figure 4.2 Sensitivity to different x_F values

where x_F is the longitudinal momentum component of the decaying particle divided by its maximum allowed value, $b = 2$ and n is kept as a variable which must be fitted. The sensitivity of this experiment to different x_F values is illustrated in figure 4.2.

(v) Semileptonic branching ratios and decay distributions. The appropriate branching ratio is 4.5% for Λ_c^+ [8], 5% for neutral D mesons [9] and we assume 10% for a mixture of charged and neutral D mesons. The decays are generated isotropically in the charmed particle rest frames with an energy distribution according to four-body phase space for the Λ_c^+ averaged over the decays to $pKe\nu$ and $\Lambda\pi e\nu$ [10]. For the neutrinos from D decays the energy spectrum is calculated from the parametrizations of Ali and Pietarinen [11], averaged over equal $Ke\nu$ and $K^*e\nu$ final states [10].

(vi) The A-dependence of the cross-section. To obtain a cross-section per nucleon, which is useful for comparisions between experiments which use different nuclear targets, we need to know whether the charm cross-section is proportional to the total inelastic cross-section for nuclear scattering ($\sigma \sim A^{\approx\frac{2}{3}}$) or to the nucleon number ($\sigma \sim A^1$). Here results are presented assuming A^1 dependence, noting that for copper the $A^{\frac{2}{3}}$ assumption gives cross-sections ≈ 3 times bigger per nucleon.

4.5.2 Fitting the data

Because of the clear excess of prompt e^- above the prompt e^+ rate, the natural choice of model is $\Lambda_c^+\overline{\mathrm{D}}$ production, with the $\overline{\mathrm{D}}$ being predominantly neutral. $\mathrm{D}\overline{\mathrm{D}}$ production cannot account for such a difference unless the n values for the spectra differ greatly, which seems not to be the case. D^- production in association with the Λ_c^+ would not reproduce the observed difference because the semileptonic branching ratio 19% [9] would favour an excess of e^+.

The prompt $e^\pm$ rates as a function of energy have been calculated by K.Hultqvist. [12] The best fit to the e^- data using Λ_c^+ spectra is obtained with $n = 2.5 \pm 0.5$ ($\chi^2_{min} \approx 14$) and is shown in figure 4.3. For the e^+ data $n = 2 \pm {}^{2}_{0.5}$ ($\chi^2_{min} \approx 2.5$), shown in figure 4.4. The corresponding cross-sections are $105 \pm \approx 30\mu$b and $16 \pm {}^{28}_{6}\,\mu$b. The cross-sections should agree, and differ here by over 2σ. Averaging these values nevertheless, we would expect a cross-section of $\approx 60 \pm 40\,\mu$b per nucleon for this interpretation. If we *require* equality in the cross-sections, sacrificing the shape of the spectrum, we could have $n = 1$

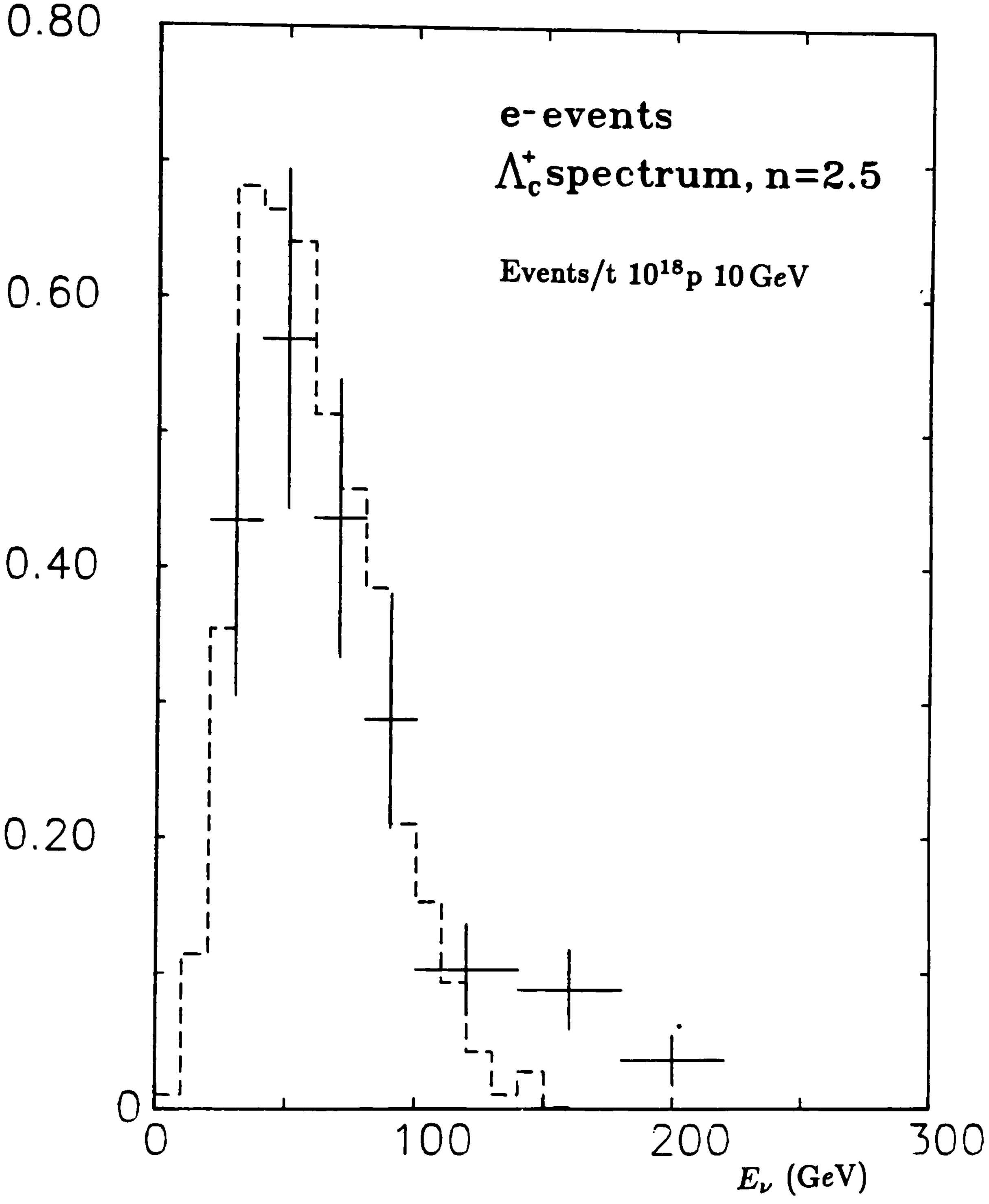

Figure 4.3 Fit to the prompt e^- rate from Λ_c^+ decay

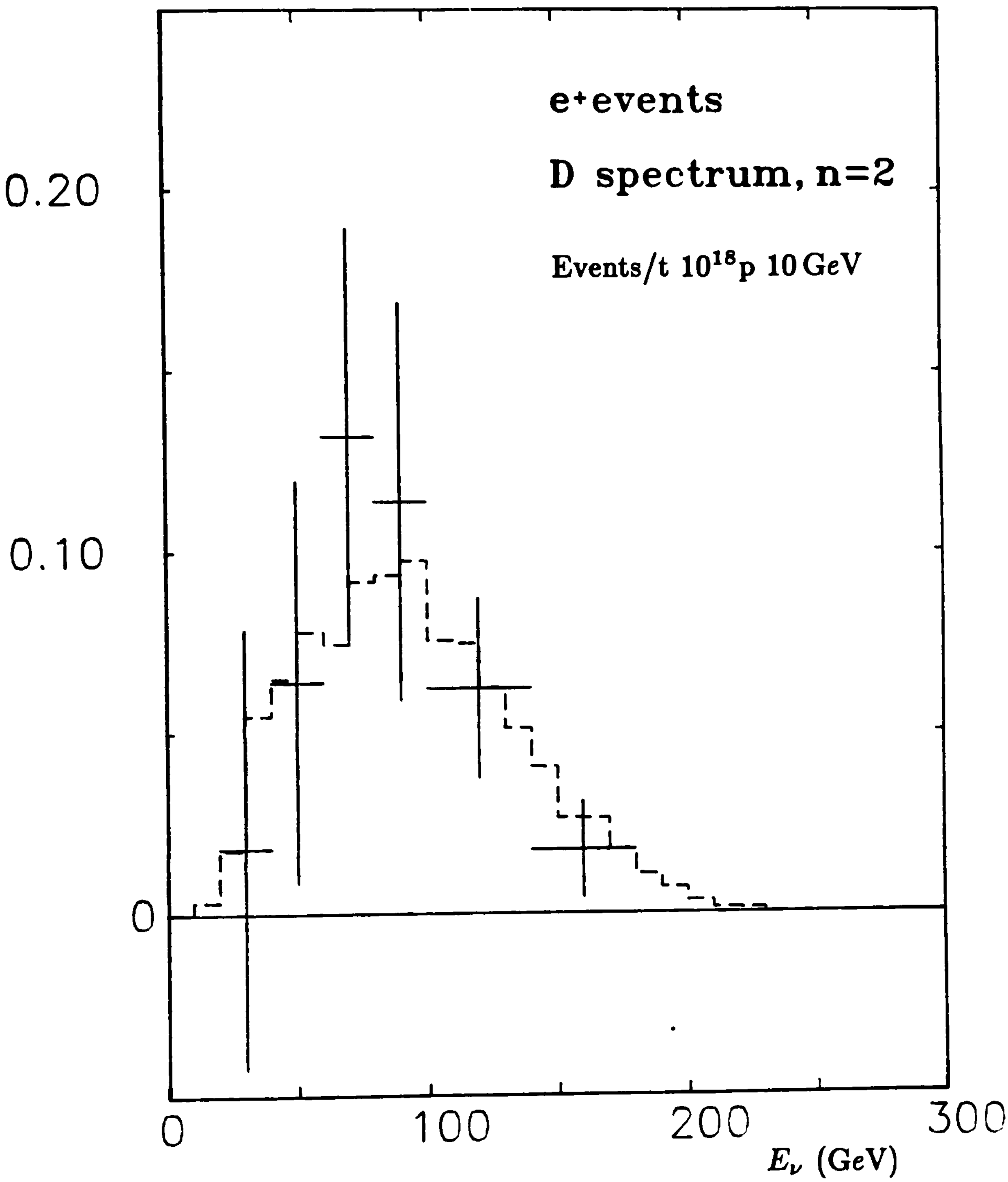

Figure 4.4 Fit to the prompt e^+ rate from D decay

for the Λ_c^+ production and $n = 3$ for $\overline{\mathrm{D}}^{\circ}$, with a cross-section of $\approx 30\mu$b per nucleon. The e^- fit in particular is poor in this case with $\chi^2 \approx 80$.

The event difference $e^- - 1.128e^+$ has been fitted by K.W.Barnham and G.Myatt,[13] the conventional signal cancelling to a good approximation (see table 4.2a). With the same basic assumptions and values of $n = 0.5$ for Λ_c^+ and $n = 4$ for $\overline{\mathrm{D}}^{\circ}$ the event difference can be reproduced, and $\sigma(\Lambda_c^+\overline{\mathrm{D}}^{\circ}) \sim 26\mu b$, adjusting the value obtained to give the result for A^1 dependence. The total e^- rate is then slightly in excess of the observed rate, and implies that this mechanism must be dominant.[13]

There is clearly no simple model which can explain the data in all respects. Analysis of the prompt far throughgoing muon signal which is in progress suggests that an asymmetry between the neutrino and antineutrino fluxes is not seen. In conclusion we note that our electron rates suggest that Λ_c^+ production may be the dominant process, with a cross-section of $16 - 105\,\mu$b per nucleon but that a model which fits both the magnitudes and the shapes of the prompt $e^{\pm}$ spectra has not been found.

References

[1] K.Hultqvist, WA66 note.

[2] H.Wachsmuth, WA66 note.

[3] H.Wachsmuth and W.Venus, WA66 note.

[4] WA66 collaboration, paper in preparation.

[5] P.C.Bosetti et al, *Physics Letters* **110B** (1982) 167.

[6] H.Wachsmuth, XXII High Energy Physics Conference. (Leipzig, 1984).

[7] P–O.Hulth, WA66 note.

[8] E.Vella et al., *Physical Review Letters* 48 (1982) 1515.

[9] Particle Data Group, *Reviews of Modern Physics* **n** (1984).

[10] G.Myatt, private communication.

[11] A.Ali and E.Pietarinen, *Nuclear Physics* **B154** (1979) 519.

[12] K.Hultqvist, private communication.

[13] G.Myatt and K.W.Barnham, WA66 note.

5

The Tau-Neutrino

Although current belief is that the tau-neutrino exists, evidence for a single unambiguous tau-neutrino interaction has yet to be seen. The expected number of tau-neutrino events in this experiment and a shape for their energy spectrum are calculated.

5.1 Introducing The Tau-Neutrino

So far the existence of the tau-neutrino (ν_τ) and its properties have been inferred in much the same way as electron-neutrinos were first deduced from nuclear beta decay by Pauli. The tau-neutrino is a neutral lepton which is expected to couple to the charged tau lepton and to carry its lepton number. This lepton number is distinct from that of the electron and muon families since the decay $\tau^- \rightarrow l^- \gamma$ would be predominant for such an assignment. It is also distinct from the anti-lepton numbers of these families, or the decay $\tau^- \rightarrow l^- \bar{\nu}_l \nu_\tau$ would proceed at a higher rate by a factor of two for the case in which the final state neutrinos $\bar{\nu}_l$ and ν_τ have the same lepton number and are therefore identical [1]. This is ruled out by the near equality of the two leptonic branching ratios for the tau. The evidence, then, is that the tau and its neutrino are sequential leptons, i.e. that they form a new lepton family with its own lepton number.

The tau-neutrino is a spin-half particle [1], and its mass is known experimentally to be less than 125 MeV at 95% CL [2] (from the decay $\tau^- \rightarrow 4\pi\ \nu_\tau$). In the following analysis, its mass is assumed to be zero.

Our first requirement is a model for the production of tau-neutrinos which can be used to predict the overall flux and its energy dependence, this being necessary for the later calculations of possible signals and their corresponding backgrounds in the search.

5.2 Tau-neutrino sources

Possible sources of tau-neutrinos in the beam dump process (p Cu$\rightarrow$X ν_τ) are heavy flavour decay (i.e. the decays of hadrons containing charmed or b- quarks) and the Drell-Yan process ($q\bar{q} \rightarrow \tau^+\tau^-$) followed by the decay of the taus. The Drell-Yan tau pair production process can be calculated [3] using measured data for muon pair production, which has a cross-section

$$\frac{d\sigma}{dQ^2} = \frac{4\pi\alpha^2}{3Q^4} f(t)$$

where Q^2 is the square of the four-momentum transfer, α is the QED fine-structure constant and $f(t)$ accounts for the quark distribution inside the proton. For tau-pair production we cannot ignore the lepton mass and threshold effects must be taken into account. The overall result is a cross-section of the order of 0.2 nbarns [3]. As for heavy flavour decay, the most probable source of tau-neutrinos must be charm, simply because the heavier flavours are produced orders of magnitudes less frequently. The D-meson is only slightly more massive than the tau lepton, and the decay is suppressed by $\sin^2\theta_c$ (≈ 0.05) from the Cabbibo mixing between the d quark and the weak eigenstate s quark. The best candidate is the F meson which is both charmed and strange and which was recently rediscovered at a mass of 1971 GeV [4]. The overall process for ν_τ production would then be

$$\mathrm{pCu} \rightarrow \mathrm{F}^{\pm} + \ldots$$

$$\mathrm{F} \rightarrow \tau^{\pm}\nu_{\tau}$$

$$\tau \rightarrow X\nu_{\tau}.$$

The cross-section for F production lies between the limits $0.1 \leq \frac{\sigma_{\mathrm{F\overline{F}}}}{\sigma_{\mathrm{D\overline{D}}}} \leq 0.5$. The lower limit is the K to π ratio [5] and is likely to be an under-estimate [6] because the pion mass is small in comparison with the kaon mass whereas the F and D masses are relatively close together. The upper limit is calculated assuming flavour SU(3) symmetry, [7] in which case we would have $\sigma(\mathrm{F}^+) = \sigma(\mathrm{D}^+) = \sigma(\mathrm{D}^\circ)$. Here we shall take $\sigma_{\mathrm{F\overline{F}}} = 0.3\ \sigma_{\mathrm{D\overline{D}}}$ and we take the $\mathrm{D\overline{D}}$ cross-section to be 20 μb per nucleon, estimated from an analysis of previous beam dump results [8]. We also require the branching ratio of the F into a tau lepton and neutrino, given by

$$\Gamma(\mathrm{F} \rightarrow \tau\nu_{\tau}) = \frac{G_{\mathrm{F}}^2}{8\pi}\ f_{\mathrm{F}}^2\ m_{\mathrm{F}}\ m_{\tau}^2\ \left(1 - \frac{m_{\tau}^2}{m_{\mathrm{F}}^2}\right)^2$$

which depends on the value of the unknown f_{F}. If we take a value of 200 MeV the result is a branching ratio of $1.7 \pm {}^{0.8}_{0.5}\%$ [9]. Putting these values together we predict $\sigma \times \mathrm{B.R.}(\mathrm{pCu} \rightarrow \mathrm{F} \rightarrow \tau\nu_{\tau}) \approx 0.4\,\mu\mathrm{b}$. This is larger than the Drell-Yan cross-section by some three orders of magnitude, and we shall take F production and decay to be our ν_{τ} source.

5.3 Production and Decay of F Mesons

We proceed to calculate the overall size and energy dependence of the ν_τ flux and the numbers and energies of events expected at BEBC. The monochromatic proton beam incident on the dump will produce a cascade of particles, and we must take into account the effects of the secondary protons produced. This has been done using two sets of experimental data. The secondary protons are generated according to the measured distribution of [10],

$$d^2N = A\left(\frac{B+1}{p_0}\left(\frac{p}{p_0}\right)^B\right)\left(\frac{2Cp^2}{2\pi}e^{-Cp^2\theta^2}\right) dp\, d\Omega$$

with $A = 0.8$, $B = -0.6$, $C = 3.5$. The expressions in brackets are normalised, so A is the average number of secondary protons per incident proton. The effective elasticity of the collision $\left(\frac{p}{p_0}\right)$ has a mean value $\frac{2}{7}$ which can be calculated from this expression by hand. The proton momenta for subsequent generations are obtained by repeating this procedure iteratively. This distribution was obtained with a beryllium target, and we use lower energy data [11] scaled up to 400 GeV to convert the spectrum of protons to that expected for a copper target. The resulting distributions for the first and second generation of secondaries are shown in figure 5.1.

The F production cross-section is taken to be proportional to $s^{1.3}$, so the low energy protons are not expected to contribute much, and only one generation of secondaires has been included in the calculation. F mesons are assumed to be produced in the copper target with a momentum distribution given by

$$E\ d^3\sigma \sim (1-|\ x_F\ |)^n\ e^{-bp_T} dx_F\ d^2p_T$$

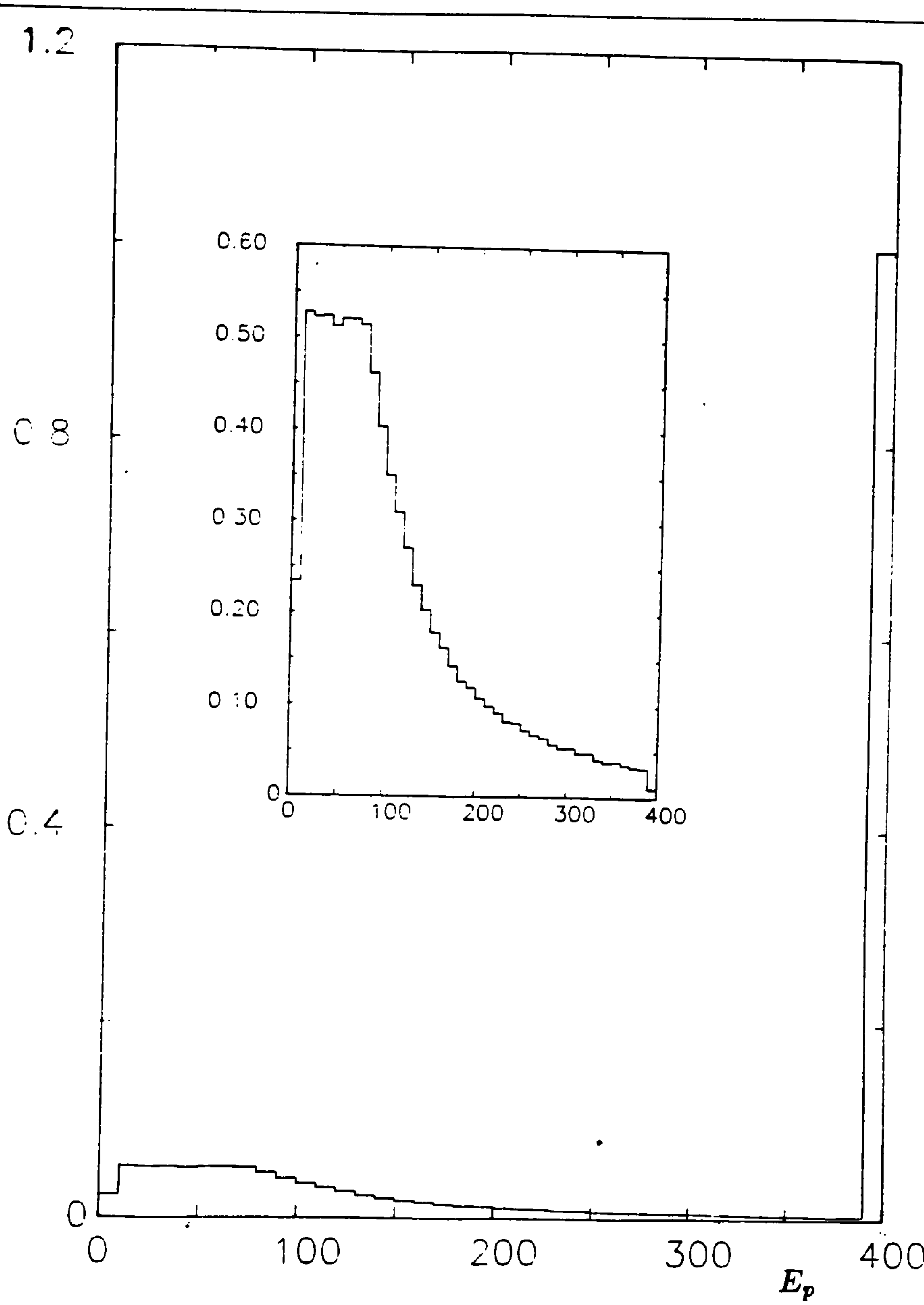

Figure 5.1 Proton cascade in the Beam Dump Target.
Distribution of proton momenta in the beam dump including one generation of secondaries. The inset shows the secondaries scaled up by a factor of ten.

Table 5.1 Branching ratios used for $\tau \to X\nu_\tau$

X	B.R.
$l\nu$	0.36
ρ	0.24
A_1	0.10
π	0.10
$n\pi$	0.20

where x_F is the ratio of the longitudinal momentum of the decaying particle in the centre of mass frame divided by the maximum value that its momentum can take. Being spin zero states, the F mesons decay isotropically in their rest frame and each of the two final state leptons has a definite momentum

$$p_{\nu,\tau} = \frac{m_{\mathrm{F}}^2 - m_\tau^2}{2m_{\mathrm{F}}} \approx 0.18\,\mathrm{GeV}$$

These decay neutrinos are seen in the flux at the low energy end of the distribution. It is important to note that the tau lepton which is produced in F decay is polarised, *against* its preferred helicity state, since it must balance both the neutrino momentum and spin. The tau lepton then decays into a final state containing another ν_τ, and there is generally much more momentum available to the neutrinos in this process, and these contribute the broad part of the neutrino spectrum and most of the events. The decay modes of the tau lepton and the branching ratios and decay distributions which were used in the calculation are summarised in table 5.1 and discussed further in appendix 1.

5.4 Decays of the Tau-lepton

It was, of course, the discovery of the tau lepton in 1975 [12] which began the search for the associated tau-neutrino. The tau was found by looking for leptonic decays in coincidence in the process

$$e^+e^- \rightarrow \tau^+\tau^-$$
$$\tau^+ \rightarrow l^+ \nu_l \bar{\nu}_\tau$$
$$\tau^- \rightarrow l^- \bar{\nu}_l \nu_\tau$$

The detailed theoretical calculation of the tau lifetime and its branching ratios can be done in the framework of V–A theory, making some assumptions about the effects of the strong interaction in the hadronic cases (i.e. using appropriate form-factors). It is interesting to note, however, that a surprisingly close approximation can be obtained by the following simple argument; the tau decay proceeds via virtual W exchange to final state $(e\nu)$, $(\mu\nu)$, $(u\bar{d})$, the other quark combinations being ruled out because of their higher masses and/or Cabbibo suppression. There being three colour degrees of freedom, the expected branching ratios are :

$$\tau \rightarrow e\nu_e \qquad 20\%$$
$$\tau \rightarrow \mu\nu_\mu \qquad 20\%$$
$$\tau \rightarrow (u\bar{d}) \qquad 60\%$$

and an estimate of the lifetime is given by assuming the width is five times bigger than the width for the decay $\tau \rightarrow e\nu_e$, say, namely

$$\Gamma = 5\,\frac{G_F^2\, m_\tau^5}{192\,\pi^3}$$
$$t(\tau) = \frac{1}{5}\left(\frac{m_\mu}{m_\tau}\right)^5 t(\mu) \quad \approx 3.2 \times 10^{-13} s$$

which agrees with measured values. In fact a similar calculation putting the measured leptonic branching ratios into the above formulæ in place of the approximation $\frac{1}{5}$ gives a value for the lifetime which has smaller errors than the direct measurements:

$t(\tau) = 2.80 \pm 0.16 \times 10^{-13}\,\mathrm{s}$, calculated,

$t(\tau) = 3.4 \pm 0.7 \times 10^{-13}\,\mathrm{s}$, measured.[13]

5.5 Kinematics of the Tau-Neutrino Interaction

Having generated the neutrino momenta, the flux is calculated by discarding neutrinos which would pass outside the angular acceptance of BEBC (±4.4 mrad). The event spectrum is obtained using

$$dN(E_\nu) = \int_0^{1.8} \phi(E_\nu, r)\, W_p\, l_{\mathrm{BEBC}}(r)\, \frac{\sigma_\tau(E_\nu)}{\sigma_\mu(E_\nu)}\, \sigma_\mu\, E_\nu\, dr$$

where ϕ is the flux, W_p is a weighting factor necessary for secondary protons, l_{BEBC} is the effective mass per unit area of BEBC at a given radius (the density of the filling being averaged over the whole run), $\sigma_\mu\, E_\nu$ is the muon-neutrino inelastic scattering cross-section, which is multiplied by an energy dependent factor in order to produce the charged current tau-neutrino interaction cross-section. This factor must be evaluated as a function of energy as the significant tau lepton mass means that the assumptions usually made in calculating the form of the cross-section for electron and muon charged currents are not valid in this case.

The details of this calculation can be found in [14], but note that this paper presents calculations for heavy gauge leptons not for conventional sequential leptons. The appropriate choice of the sign of F_3 can be checked by ensuring that the usual form for the cross-sections is obtained in the limit $m_\tau \to 0$. For massive lepton production one has the cross-section

$$\frac{d^2\sigma_\nu^{\bar\nu}}{dx\,dy} = f(E_\nu,y)\frac{G_F^2 M E_\nu}{\pi}\left\{\left(xy+\frac{m_\tau^2}{2ME_\nu}\right)yF_1+\left(1-y-\frac{M}{2E_\nu}xy+\frac{m_\tau^2}{4E_\nu^2}\right)F_2\right.$$
$$\left.\pm\left(xy\left(1-\frac{y}{2}\right)-\frac{m_\tau^2}{4ME_\nu}y\right)F_3+\frac{m_\tau^2}{M^2}\left(\left(\frac{M}{2E_\nu}xy+\frac{m_\tau^2}{4E_\nu^2}\right)F_4-\frac{M}{2E_\nu}F_5\right)\right\}$$

The five structure functions are related and we approximate $2xF_1 = F_2$, $-xF_3 = F_2$, $F_4 = 0$ and $xF_5 = F_2$. The function $F_2(x)$ is parametrized with a polynomial in $(1-x)$, the coefficients being given by the authors. Note that one of the parametrizations given by the authors contains a misprint, as the coefficients of $(1-x)$ do not add up to the value at $x=0$ implied by the accompanying figure. The factor $f(E_\nu,y)$ accounts for kinematic suppression above the threshold energy

$$E_\nu^{min} = \frac{m_\tau^2+2m_\tau M}{2M} \approx 3.5\,\mathrm{GeV}$$

corresponding to the quasi-elastic process $\nu_\tau N \to \tau N'$. In the derivation of the usual cross-section for light lepton production, we have the phase space term [15]

$$\frac{d^3p_l}{E_l} = \frac{p_l^2}{E_l}dp_l\,d\Omega = \frac{p_l}{E_l}E_l\,dE_l\,d\Omega.$$

For the muon $p_\mu \approx E_\mu$ and this leads to the usual form for the muon cross-section. For the tau lepton this approximation is not valid and we have the extra term

$$f(E_\nu,y) = \frac{p_\tau}{E_\tau} = \left(1-\frac{m_\tau^2}{E_\nu^2(1-y)^2}\right)^{\frac{1}{2}}$$

The production is also kinematically constrained to lie within the limits:

$$\frac{m_\tau^2}{2M(E_\nu-m_\tau)} < x < 1$$

$$A - B < y < A + B$$

where A and B are given by

$$A = \frac{1}{2}\left(1 - \frac{m_\tau^2}{2ME_\nu x} - \frac{m_\tau^2}{2E_\nu^2}\right)\left(1 + x\frac{M}{2E_\nu}\right)^{-1}$$

$$B = \frac{1}{2}\left(\left(1 - \frac{m_\tau^2}{2ME_\nu x}\right)^2 - \frac{m_\tau^2}{E_\nu^2}\right)^{1/2}\left(1 + x\frac{M}{2E_\nu}\right)^{-1}$$

The allowed kinematic region is shown in figures 5.2 and 5.3 and the ratio of the tau-neutrino cross-section to the muon-neutrino cross-section taking all the above effects into account is plotted in figure 5.4.

5.6 The Expected Rate—Result

Putting in the best possible values for the parameters b and n in the F decay ($b = 2$, $n = 3$ is a popular choice being a reasonable fit to the available charm production data) and the estimated F production cross-section and branching ratio and measured muon-neutrino and antineutrino cross-sections [16] the predicted number of events in BEBC is 7.54 ($2.85\,\tau^-$, $1.59\,\tau^+$, 3.1 NC) for the whole run. The energy dependence of the flux and events has been calculated and is shown in figures 5.5, 5.6. The factors affecting the shape of the distribution are comparatively well known, and in most of the calculations it is sufficient to use this shape without normalisation as we can often quote expectations per tau-neutrino interaction.

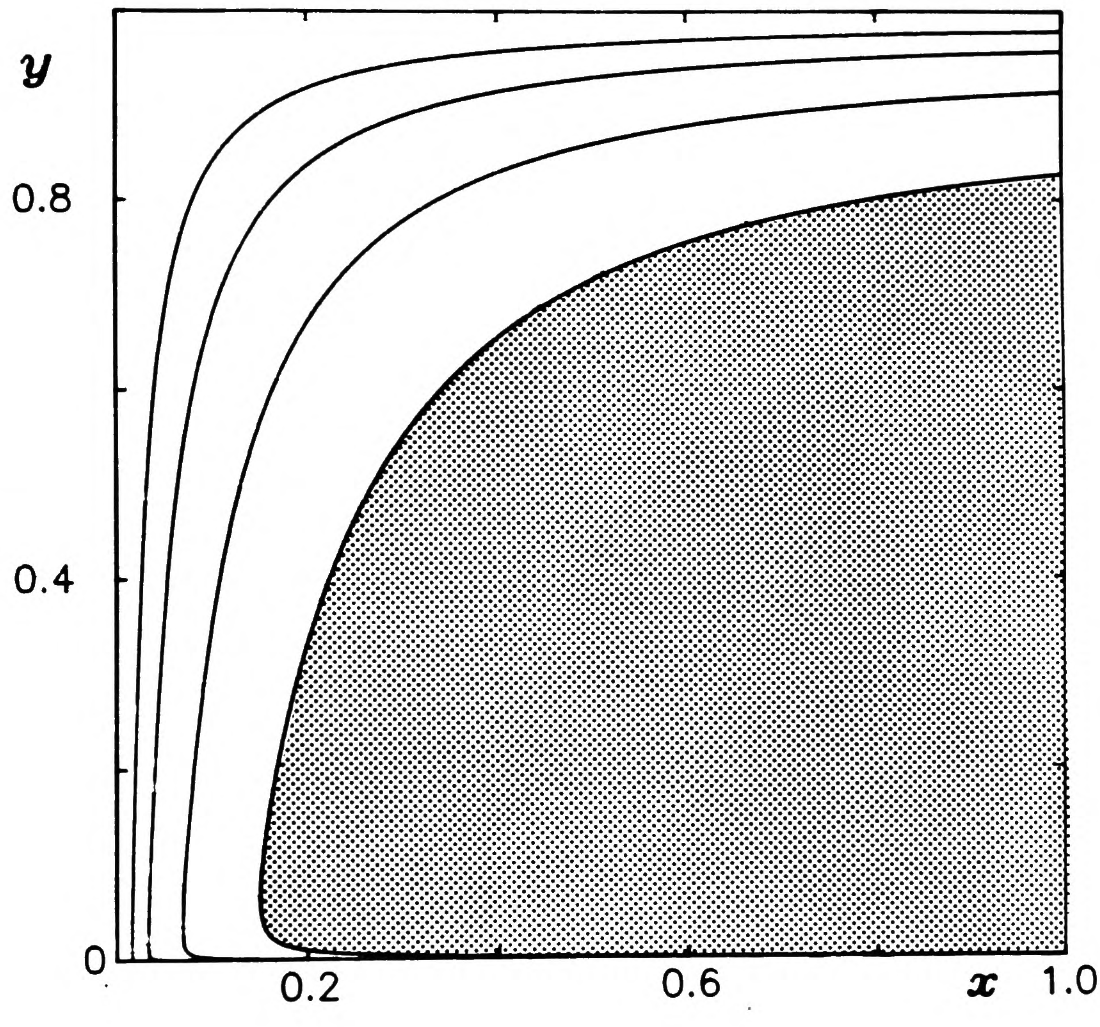

Figure 5.2 Kinematically allowed region for CC tau-neutrino interactions
The allowed regions for neutrino energies of 12.5, 25, 50 and 100 GeV.
As the energy tends to infinity the allowed region fills the x-y plane.
The shading shows the allowed region for a 12.5 GeV neutrino.

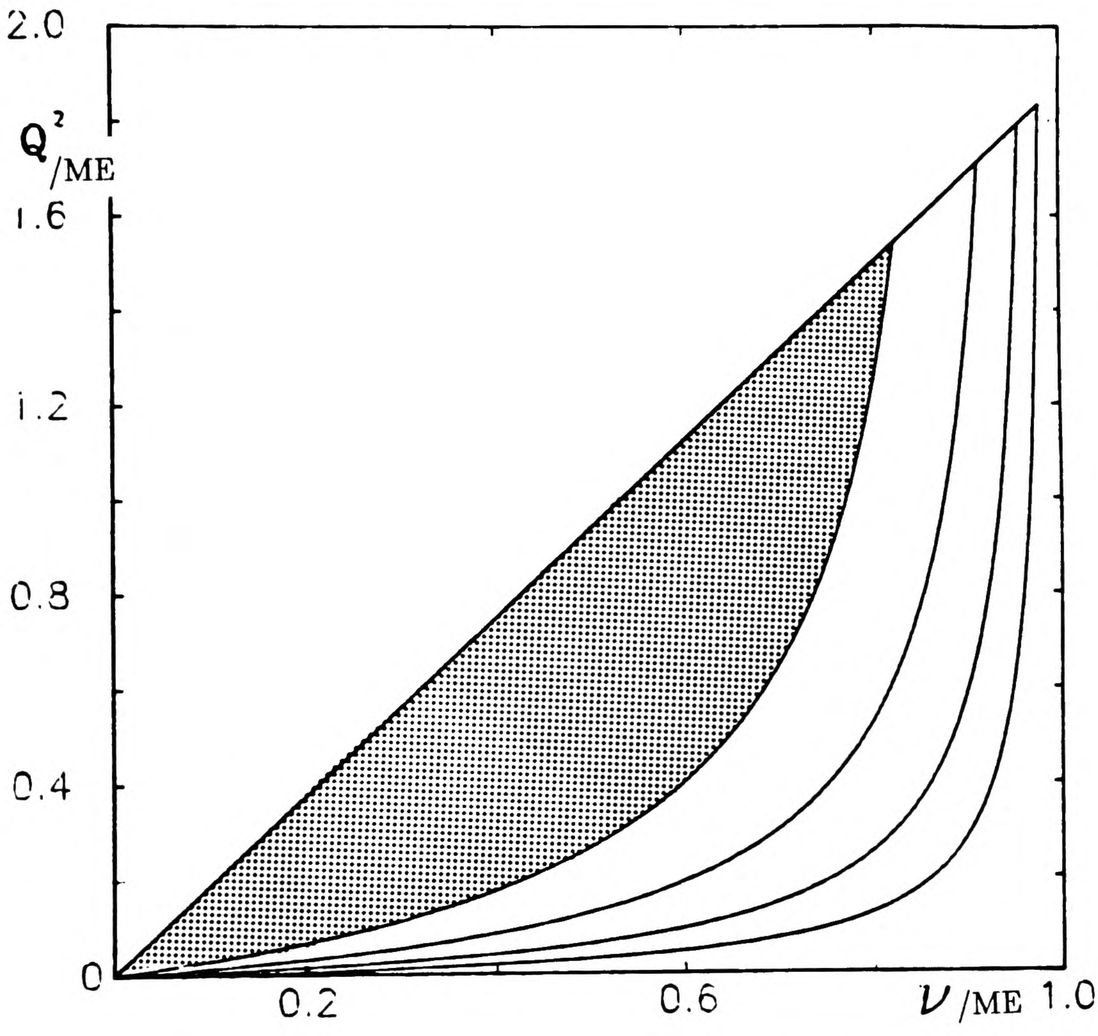

Figure 5.3 Allowed region in ν/ME and Q^2/ME
The allowed region of $\nu - Q^2$ space for tau-neutrino energies of 12.5, 25, 50 and 100 GeV. For light leptons the region is bounded by $\nu = 1$, $Q^2 = 0$ and $Q^2 = 2M_p\nu$. The allowed region for a 12.5 GeV tau-neutrino is shaded

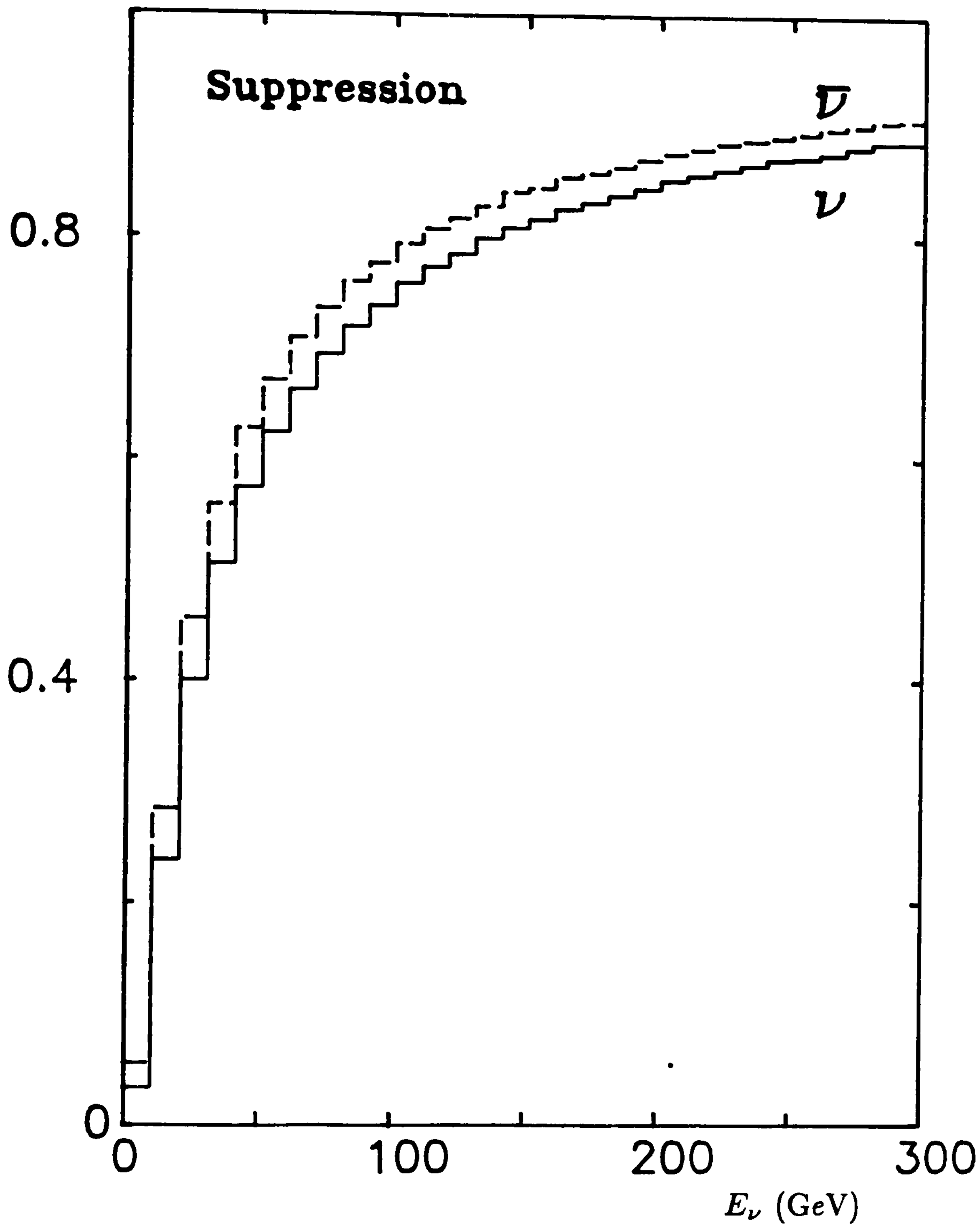

Figure 5.4 Suppression of Charged Current Tau-neutrino Interactions
The ratio of the charged current cross-section for taus to that for muons obtained by integrating the cross-sections over x and y as a function of energy

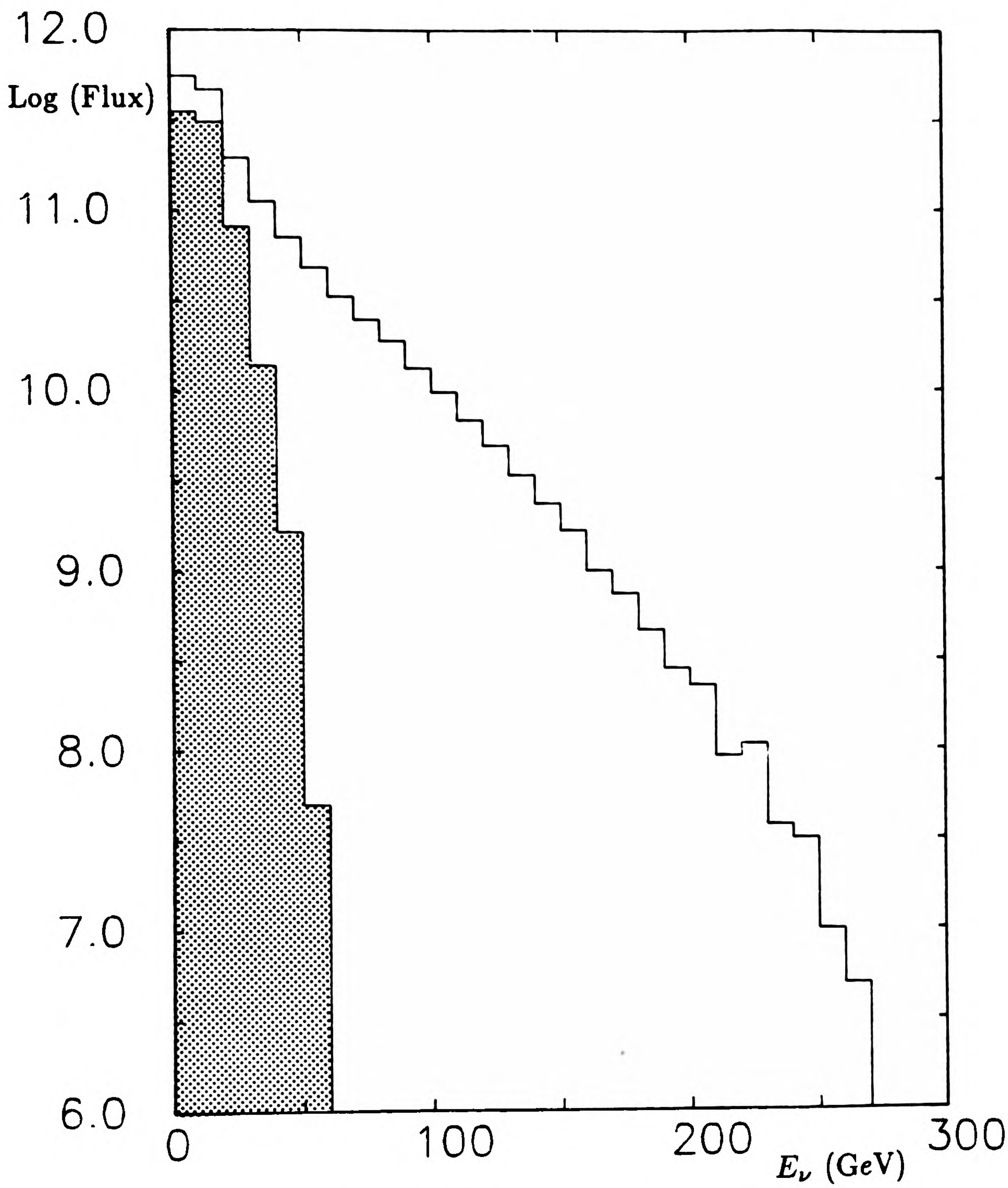

Figure 5.5 Tau-neutrino Flux

Logarithm of tau-neutrino flux expected per 10^{14} F decays to $\tau\nu_\tau \ldots$

The shaded part is from the decay $F \rightarrow \tau\nu_\tau$

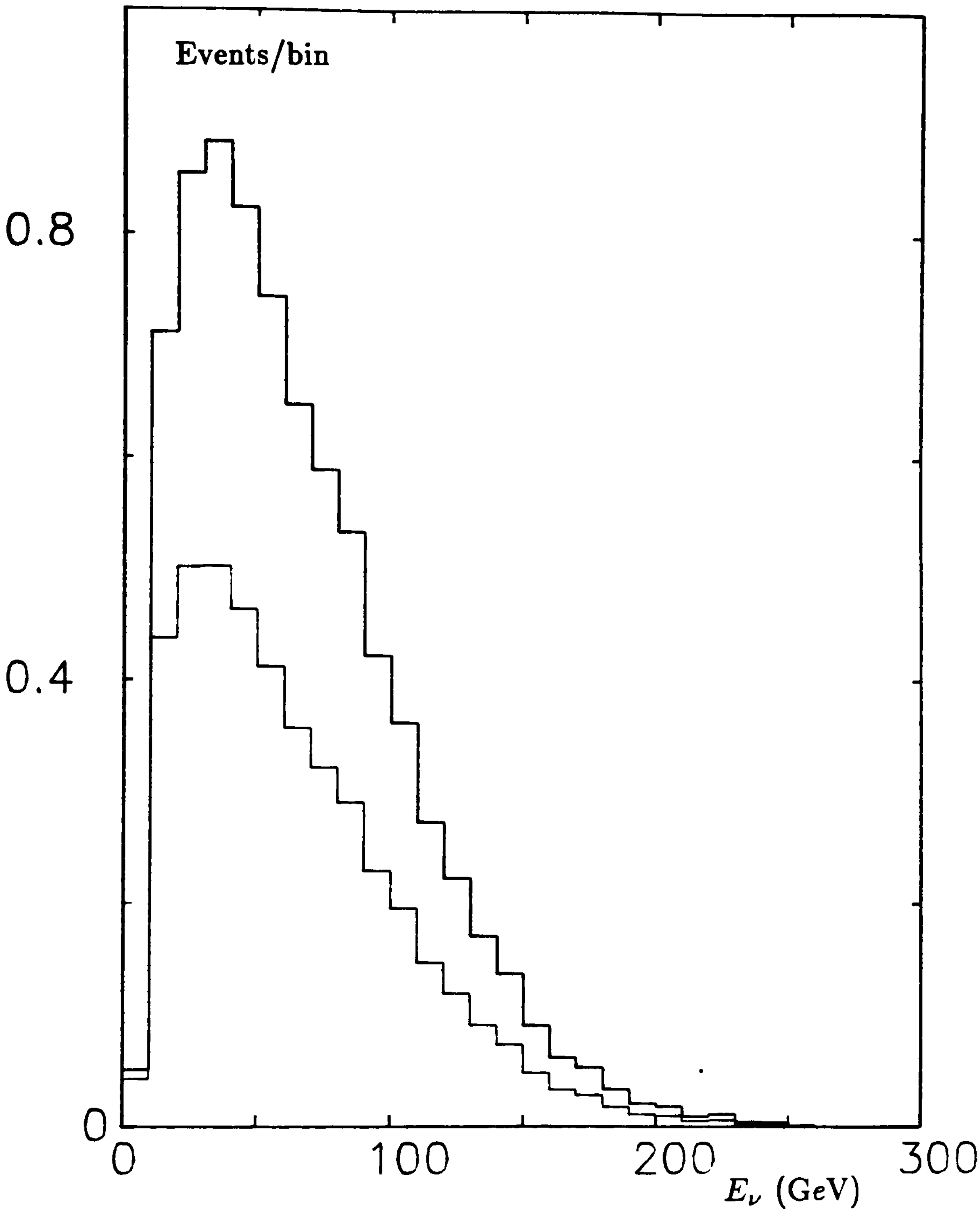

Figure 5.6 Tau-neutrino and Antineutrino Events

τ^- and τ^+ events expected per 10^{14} F decays to $\tau\nu_\tau$...

References

[1] Y.S.Tsai, SLAC-PUB 2105 (1978)

[2] P.R.Burchat et al., SLAC-PUB 3602 (1985)
C.Matteuzzi et al., SLAC-PUB 3560 (1985)

[3] M.Poppe, D.Phil thesis, Oxford (1981).

[4] R.Galik, CLEO-83/08 (1983).

[5] F.Sciulli in *Proceedings, 1978 neutrino conference (Purdue)* (1978)

[6] C.H.Albright, R.Schrock and J.Smith, *Physics Review* **D20** (1979) 2177.

[7] E.L.Berger, L.Clavelli and N.R.Wright, *Physics Review* **D27** (1983) 1080.

[8] A.Kernan and G.VanDalen, *Physics Reports* **106** (1984) 297.

[9] A.de Rujula and R.Ruckl, *Proceedings of the SSC fixed target workshop* (1984) 33.

[10] H.Atherton et al, CERN yellow report 80–08 (1980).

[11] T.Eichten et al, *Nuclear Physics* **B44** (1972) 333.

[12] M.Perl et al, *Physics Review Letters* **35** (1975) 1489.

[13] Particle Data Group, *Reviews of Modern Physics* **56** (1984).

[14] C.H.Albright and C.Jarlskog, *Nuclear Physics* **B84** (1975) 467.

[15] S.M.Bilenky, *Introduction to the Physics of Electroweak Processes* (Pergamon, 1982).

[16] P.C.Bosetti et al, *Physics Letters* **110B** (1982) 167.

6

Visual Search For Tau-Neutrino Interactions

The most compelling evidence for a tau-neutrino signal would be a photograph of an event where the tau lepton produced could be positively identified by its decay. The scans for tau-neutrino interactions in this experiment are described. One candidate event was found and this is described in detail to illustrate the problems encountered in deciding what a possible tau-neutrino interaction may be attributed to.

6.1 Scanning for Tau-Neutrino Interactions

Three separate searches for visual evidence of a tau-neutrino interaction were performed in this experiment; all the charged current events were inspected on the four normal camera views and all events which were visible on the high resolution camera were examined. Two samples of kinematically selected events were also scanned.

6.1.1 Scanning film from The high resolution camera

This extra camera situated in BEBC camera port 1 has a resolution of about $200\,\mu$ on axis and gives a useful magnification around three times that of the standard cameras. Unfortunately the angular acceptance and field of view are reduced and only a fraction of the fiducial volume is visible. By measuring fiducial marks on the BEBC wall which were seen at the edge of each view 1 photograph, the cone of view could be constructed and by looking at a sample of the film on which there were events with measured vertices, the useful depth of field was also determined. A program was written and circulated to the participating laboratories so that any physicist could discover if a high resolution picture of a selected event was likely to be available.

Each laboratory scanned all of its high resolution film looking at all frames on which there was known to be an event. The number of the events which were found to be clear on this view was 295 out of 2653 (11.1 %). Each vertex was inspected for tau decay signatures, i.e. for one track with a kink or a group of three tracks which do not meet at the primary vertex defined by the remaining tracks. One candidate of the latter type is shown (figure 6.1), which is an example of what we might have expected from $\tau \rightarrow 3\pi\ \nu_\tau$. In fact the

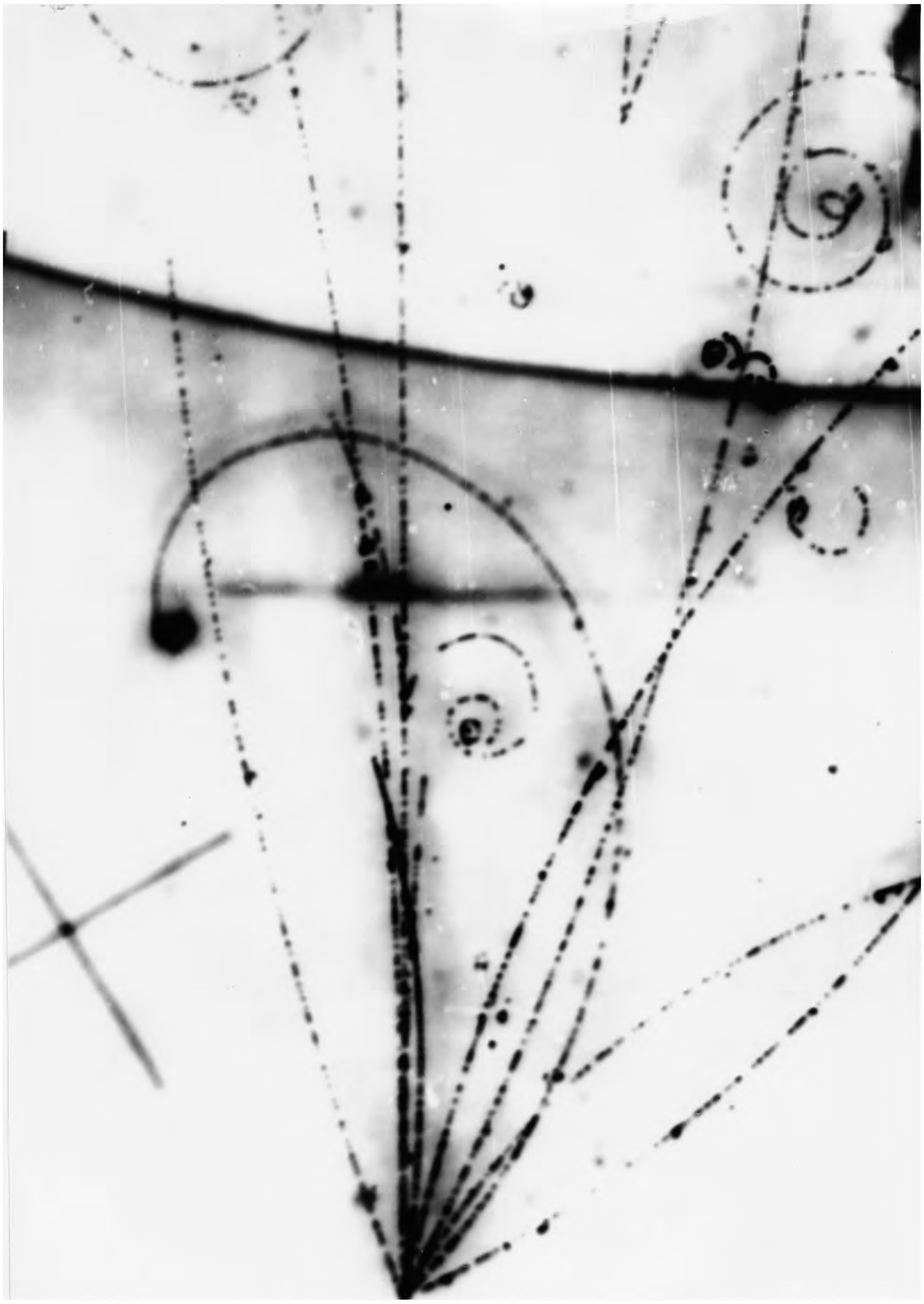

Figure 6.1

High Resolution Camera picture–Fake 3-prong decay invariant mass of the outer two tracks (0.508 GeV) is almost exactly the K° mass and the event is interpreted as an imposter, with a V° configuration sitting on top of a track from the primary vertex. Another K° decay is seen on this frame which confirms the hypothesis; it must be associated production.

6.1.2 Scanning kinematically selected events

Events were selected using criteria suggested by the tests discussed in the next chapter (sections 7.3, 7.4) and roll–frame numbers of the selected events were circulated to each of the laboratories. The frames were individually inspected by a physicist. The candidates tended to be high multiplicity events in which the region close to the primary vertex is confused. No evidence of a tau decay was seen.

6.1.3 Scanning charged current events

Using the film from the four standard BEBC cameras all events with an identified lepton in the final state were examined. Particular attention was paid to the region within 10 cm in space of the primary vertex to see if the lepton came from a decay. This meant looking for a lepton track which extrapolates wide of the vertex defined by the other charged tracks. It is thought that the eye can detect impact parameters (defined in section 6.5) of half a track-width or more, which corresponds to 250 μ in this experiment. Again it should be noted that many of the events, particularly high multiplicity events, cannot be scanned in this way as the tracks overlap in the region of interest, obscuring any kinks which there might be.

One candidate was found during this search, an event with a kink close to the vertex on a final state e^+ track, BEBC roll 974 frame 5628. The event is shown in figure 6.2. The background processes and the probability of observing an electronic tau decay are calculated, and whether this particular event can be interpreted as a tau-neutrino event is the subject of the rest of the chapter.

6.2 Interpretations

6.2.1 Possibilities

We calculate the rates for possible backgrounds which could account for this kink track and compare them with the expectation for tau decay. The possible explanations are:

(i) The event is a tau-antineutrino CC interaction with the tau decaying to an electron and two neutrinos (section 6.2.2).

(ii) The event is an electron-antineutrino CC interaction where the positron has been Coulomb scattered in the chamber (6.2.3).

(iii) The event is a muon-antineutrino CC interaction where the muon has decayed to a positron and two neutrinos (6.2.4)

(iv) The event is a neutral current or hadronic interaction and the positron comes from a hadron decay. (6.2.4, 6.2.5)

Although this event happens to contain a positron, we shall calculate the expected numbers of positrons plus electrons produced with a visible impact parameter, without

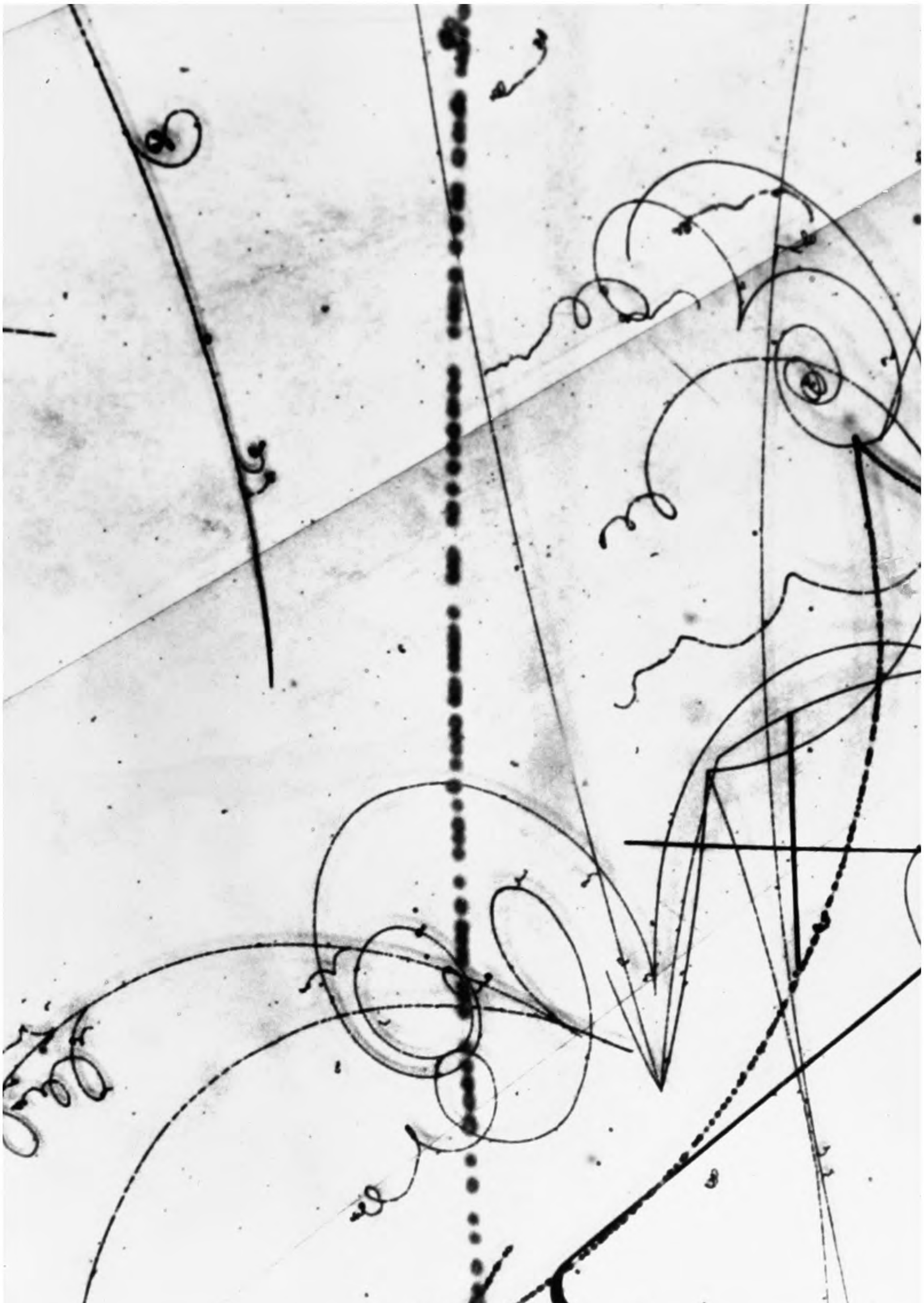

Candidate tau-neutrino event
Can *you* see a kink ?
Scale: Short proton track is 4.7 cm

biassing the tau signal to background by making favourable cuts on the distances involved. The expected signals below are all calculated with a cut of 2 cm in distance travelled by the decaying particle and for an impact parameter of 250 μ or more. The impact parameter cut corresponds to the minimum visible value and the distance cut is long enough not to reduce the signal from short-lived particles. For long lived particles we note that the expected signal is approximately proportional to the maximum allowed length.

6.2.2 The signal from tau-neutrinos

Tau lepton momenta are generated by integrating numerically over the neutrino spectrum and the expected y-distribution for tau production (section 5.5). The taus decay with an exponential distribution in space, and the electronic decay (B.R. 16.5 %) is modelled using the usual distribution in energy and angle (see eg. Appendix 1). The expected signal is 0.019 ± 0.005 (0.017 ± 0.008) events detected per charged current τ^- (τ^+) in the data. Multiplying by the expected event numbers from chapter 5, we expect 0.08 events in the $e^{\pm}$ sample, with a large error from the absolute normalisation of the event rate.

6.2.3 The signal from scattering

Multiple small-angle scattering can only account for a tiny impact parameter. We consider instead the probability of one large-angle Coulomb scatter. The cross-section for Coulomb scattering in a length dx of a medium with n scatterers per unit volume is expressed as the rate of loss $\frac{dN}{N} = -n\sigma_1 dx$ where σ_1 is the cross-section for scattering off one particle in the medium. Using parameters from [1],

$$\sigma_1(E) = \left(\frac{Z\alpha}{2E}\right)^2 \int \frac{\cos^2\left(\frac{\theta}{2}\right)}{\sin^4\left(\frac{\theta}{2}\right)} F^2(q^2) \frac{1}{1+\frac{2E}{M}\sin^2\left(\frac{\theta}{2}\right)} 2\pi \, d\cos\theta$$

where we have Z=10 for Neon, $\alpha = \frac{1}{137}$, E is the electron energy and M the proton mass, and the limits of integration over the scattering angle θ at a given distance after production depend simply on the minimum and maximum acceptable impact parameter; $q^2 = 2E(1-\cos\theta)$ is the invariant four-momentum transfer in the process; The form factor is

$$F(q^2) = \int_0^\infty \rho(r) \frac{\sin(qr)}{qr} 4\pi r^2 \, dr$$

and the nuclear charge density

$$\rho(r) = \frac{3}{4\pi c^3} \frac{1}{1+\left(\frac{\pi z}{c}\right)^2} \left(\frac{1}{1+\exp(\frac{r-c}{z})}\right)$$

The first constant is the normalisation, $c = 1.1\,Z^{\frac{1}{3}}$ is the nuclear radius at half density, $z \approx 0.5$ fm is the surface thickness and r is the distance from the nuclear centre. The probability of one positron or electron giving a visible impact parameter is very small, (9×10^{-5} for a 4 GeV particle scattering within 2 cm). Summing over the electron and positron sample as a whole, the expected rate is 4.1×10^{-3} visible scatters.

6.2.4 The signal from non-charmed particle decays

The possible particle decays which include an electron or positron plus neutrals in the final state [2] are summarised in table 6.1. The decays are discussed in order of parent particle mass.

Muon and Pion decays

A hand estimate shows that we expect of the order of $\frac{1}{\gamma}$ 3×10^{-5} decays from one muon in 2 cm and the tiny available P_T means that the acceptance for a significant impact parameter is very small. Computation of this signal gave a result of zero. For pions the small available P_T, the branching ratio to electrons and the long decay length mean that the expected rate is again negligible.

Kaon decay

To calculate the signal from kaon decay we require the number of kaons and their energy distribution as input. We assume that one tenth of the charged particles in the neutral event sample are kaons and that their energy distribution is the same as for the pions. For each kaon the decay is given a flat distribution in space and the final state electron has a spectrum in the kaon rest frame given by [3]

$$d\Gamma = \frac{(1-x)^2 x^2}{1.087 - x}\, dx\,, \qquad 1.087 = \frac{m_{\rm K}^2}{m_{\rm K}^2 - m_\pi^2}$$

where x is the energy of the electron divided by its maximum allowed value 227.1 MeV. The calculated rate in this experiment is then 1.4×10^{-3} visible decays.

Table 6.1 Stable Particle Decays to Electrons

X	m_X GeV	Decay $X \rightarrow$	BR	$c\tau$ cm
μ	0.106	$e\nu\nu$	1.0	6.59×10^4
π	0.140	$e\nu$	1.2×10^{-4}	7.80×10^2
K	0.494	$\pi^\circ e\nu$	4.8×10^{-2}	3.71×10^2
Σ^+	1.189	$\Lambda^\circ e^+ \nu$	2.0×10^{-5}	2.40
τ	1.784	$e\nu\nu$	1.7×10^{-1}	0.010
D	1.869	$K^\circ e\nu$	$\leq 1.9 \times 10^{-1}$	0.028
Λ_c^+	2.282	$e^+ \nu + \ldots$	$\leq 2.7 \times 10^{-2}$	0.007
p	0.938	$e^+\pi^\circ$	?	$\geq 1.0 \times 10^{50}$

Sigma decay

Let us generously assume that there are 100 Σ^+ in our neutral current sample. The branching ratio then implies that there will be $\sim 10^{-3}$ electronic decays. The small available P_T (71 MeV) means a very small probability of producing a visible impact parameter, although the lifetime is favourable. Certainly we expect fewer than 10^{-3} decay electrons from this source.

6.2.5 Expected signal from charmed particle decays

We now consider the interpretation of the event as a neutral current event in which a charm-anticharm pair was produced and one of the particles decayed with a visible semileptonic decay. To calculate the signal, we use an experimental observation of a charm pair in a neutral current event from an emulsion experiment [4]. The quoted rate of charm pair production per neutral current interaction is estimated as $0.6 \pm ^{1.5}_{0.3}\%$. The energies of the charmed particles are assumed to have the same spectrum as the charged particles seen in the neutral current sample. The result is not sensitive to the spectrum. The decays are modelled with the same lepton energy spectrum as in chapter 4. The appropriate semileptonic branching ratio is that to a final state where any hadrons present must be neutral, which is calculated from the data given in [2]. Assuming the charged D decays 50% to $\overline{K}^{*\circ} e\,\nu$ and 50% to $\overline{K}^{\circ} e\,\nu$ we find that a fraction 0.44 of the final states containing electrons also contain no other charged particles and no other identifying features such as 2-prong neutral decays. We assume also that the other charmed particle is not identified. If the charmed particles produced are all Ds with equal charged and neutral states, the

Table 6.2 Summary of the possible signals

Process	Events	Comment
$\tau \rightarrow e\nu\nu$	0.08	Estimate
D $\rightarrow$ (had)$^\circ e\nu$	0.11	Estimate
e scatter	4.1×10^{-3}	Estimate (per cm space)
K $\rightarrow \pi^\circ e\nu$	1.5×10^{-3}	Estimate (per cm space)

estimated number of background events is 0.11, with a large uncertainty in the charm production rate. Charmed baryon decays would reduce this estimate significantly because of the shorter lifetime and smaller P_T in the decays.

The results of the background calculations for the more probable of the signals are summarised in table 6.2.

6.3 Description of the Candidate Event

The primary vertex ($x = -149.5$, $y = 51.6$, $z = 45.3$) is within 30 cm of the upstream BEBC wall, leaving a long path in which to detect neutral particles. There are four charged tracks at the primary vertex—a short proton track, two hadronic tracks which interact in the chamber (one of each sign) and a positron identified by brems and rapid energy loss. The positron has a kink very close to the primary vertex. Five gamma conversions and a Compton electron originate in the region near the primary vertex, and there is a one-prong interaction of a neutral particle which also has a pointing Compton electron. The measurement results are summarised in table 6.3.

6.4 Further Investigation

We see that charm production cannot be neglected as a background for a tau signal. We therefore proceed to investigate the event in more detail to see if the charm interpretation can work. It is of course not possible to fit the mass of the particle which decayed to an electron since there is a missing neutrino, and we can certainly find combinations of particles with the positron which have invariant masses less than the D mass. We attempt to find a fit to the second charmed particle, which must be a D^- or $\overline{D}^{\circ}$. Firstly note the π° combinations found by combining gammas. $\gamma_F\ \gamma_S$ have an invariant mass of 138 ± 20 MeV and $\gamma_{KA}\ \gamma_{PB}$ an invariant mass 138 ± 25 MeV. They are referred to as π°_A and π°_B respectively. The following combinations are compatible with the D mass:

I	$K^- \pi^+ \pi^{\circ} \pi^{\circ}$ $(h^- h^+ \pi^{\circ}_A \pi^{\circ}_B)$	1.782 ± 0.396
II	$K^+ \pi^- \pi^{\circ}$ $(h^+ h^- \pi^{\circ}_A)$	1.723 ± 0.185
III	$K^+ \pi^- \pi^{\circ} \pi^{\circ}$ $(h^+ h^- \pi^{\circ}_A \pi^{\circ}_B)$	1.942 ± 0.381

The event is therefore compatible with charm production though none of the mass fits are convincingly close to the D mass. The conclusion, then, is that although the event has a

Table 6.3 Measurement data for Candidate Event

Particle	Type	Momentum GeV	Dip mrad	Phi mrad
e^+	positron	4.000 ± 1.200	$-\ 35 \pm 04$	307 ± 07
h^+	Interaction	0.531 ± 0.058	-257 ± 11	48 ± 15
h^-	Interaction	1.536 ± 0.194	294 ± 04	5816 ± 01
p	proton	0.368 ± 0.103	-330 ± 30	877 ± 01
n^*	Interaction	0.384 ± 0.023	-463 ± 20	310 ± 20
γ_T	Compton e	0.079 ± 0.018	892 ± 9	5390 ± 43
γ_S	gamma	0.266 ± 0.095	440 ± 48	732 ± 73
γ_R	gamma	0.368 ± 0.060	81 ± 16	6251 ± 33
γ_{KA}	gamma	0.483 ± 0.093	$-\ 63 \pm 13$	6105 ± 27
γ_{PB}	gamma	1.665 ± 0.478	. 58 ± 20	6200 ± 21
γ_F	gamma	0.084 ± 0.014	86 ± 47	6082 ± 68

reasonable interpretation as a tau-neutrino decay, the background from charm semileptonic decays is very difficult to separate.

6.5 Impact Parameter Measurement

6.5.1 Introduction

To complete the measurement data, we need to investigate the kink on the positron track. In particular we measure the impact parameter of the outgoing track, defined as the distance of closest approach to the primary vertex of the line constructed by extrapolating the outgoing track from the kink. The impact parameter is useful as its distribution is independent of the gamma factor of the decaying particle and because we can use points *beyond* the supposed kink, thereby ruling out (or not) the possibility that the effect is a distortion.

6.5.2 Measurement of the Impact parameter—Results

A program suitable for fitting measured points and extrapolating tracks close to the primary vertex had already been written in Oxford by Nick West and is described in detail by P. Cartwright,[5] whose measurement rules were adopted, namely

(i) Measure on all four views.

(ii) Measure up to approximately 60 cm of track, 50 points per track.

(iii) Measure a high density of points near the primary vertex.

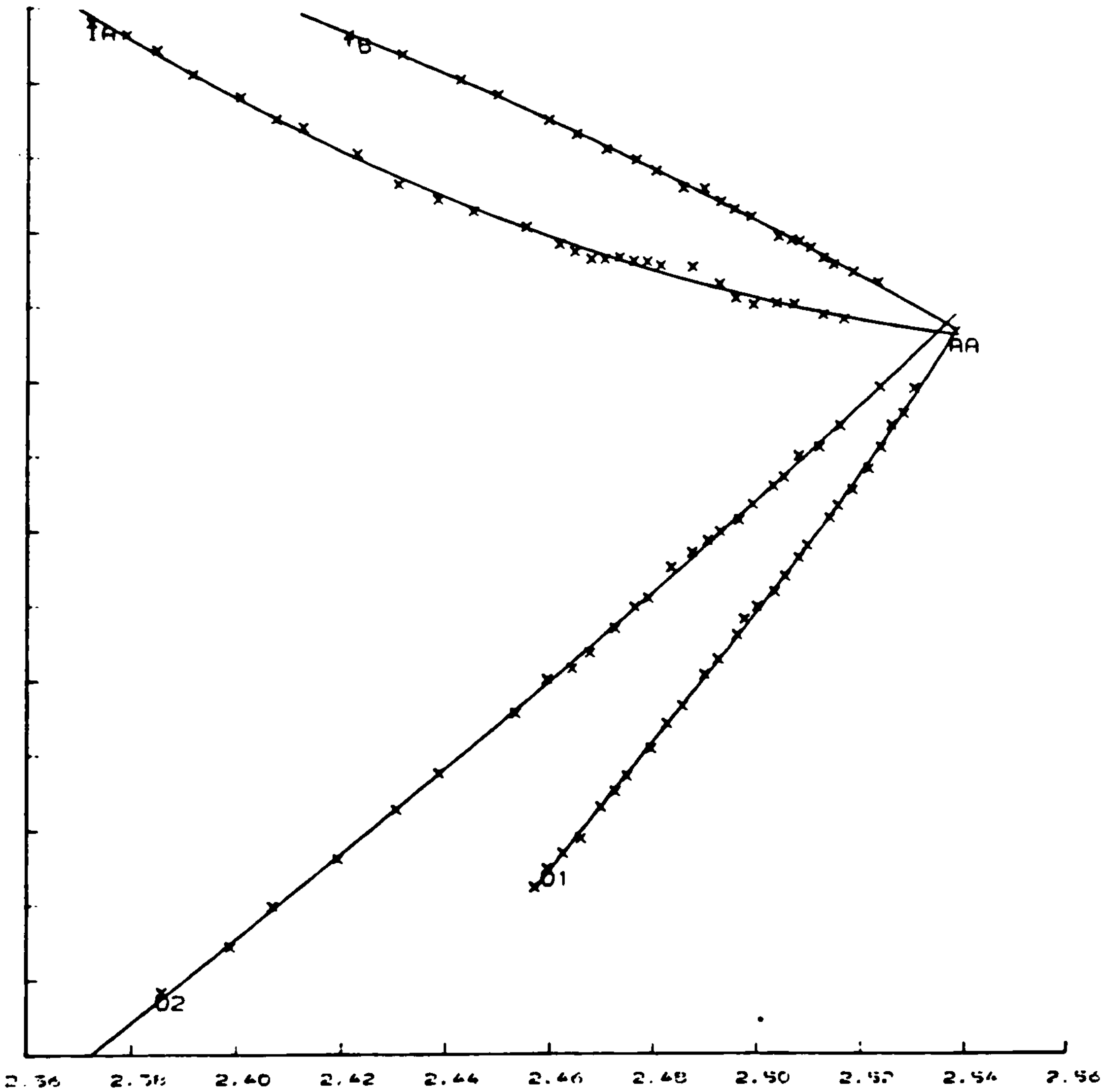

Figure 6.3 Track Measurements and 3rd order polynomial fit

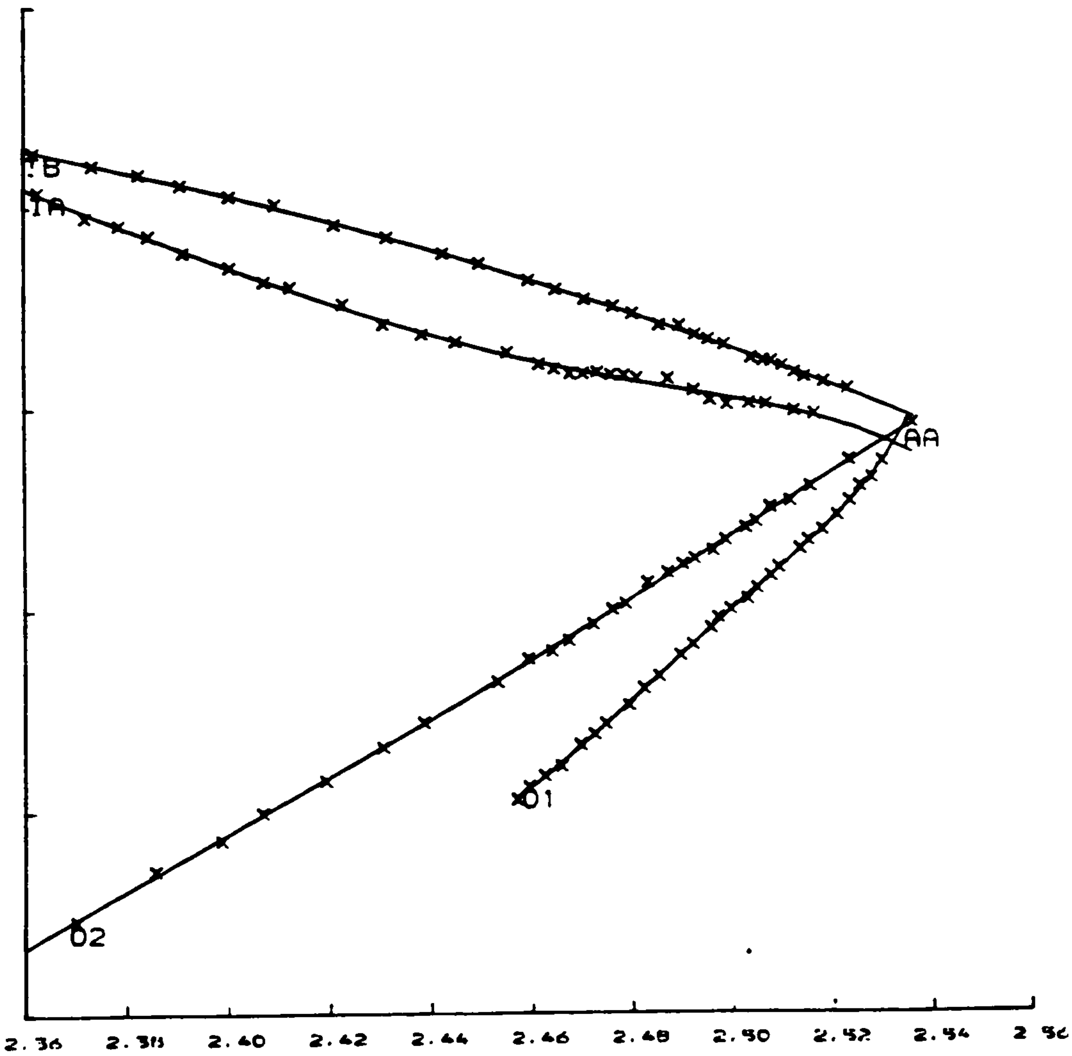

Figure 6.4 Track Measurements and 5th order polynomial fit

(iv) Do not measure where tracks are confused.

(v) Do not use computer aided track following.

After following this procedure, the analysis program was used to fit the tracks and measure impact parameters. The measurement errors here are 1–2μ on each point, about five times smaller than acceptable errors for standard measuring. An impact parameter was found on view 2 only, with a value of $\approx 12\,\mu$ on film, when fitted with a second or third order polynomial as shown, but the value is close to zero for a fourth or fifth order polynomial. The higher order fits follow the errant points on the tracks perhaps a little too well, but we must conclude that there is not a significant impact parameter for this track. The measured points and fitted third and fifth order tracks are shown in figures 6.3 and 6.4. Measurements of the distance from the kink to the primary vertex vary from 0.5–1.3 cm in space.

6.6 Conclusions

As a note for future tau-neutrino searches we see that there are two problems which need to be solved; the optical resolution needs to be very good and the bubble size small in order to improve the tau signal and to have a better chance of measuring impact parameters; the background from other processes means that accurate measurements, in particular to associate neutrals to the primary or to the kink vertex, are required. Here the uncertainties in the impact parameter measurement and in the possible origin of some of the neutrals means that we cannot finally decide what the interaction was. For these reasons, we may not interpret this interaction as evidence for tau-neutrino production in this experiment.

References

[1] F.Scheck, *Leptons, Hadrons and Nuclei* (North-Holland, 1983).

[2] Particle Data Group *Reviews of Modern Physics* **56** (1984).

[3] L.B.Okun, *Weak Interactions of Elementary Particles* (Pergamon, 1965).

[4] N.Ushida et al., *Physics Letters* **121B** (1983) 287.

[5] P.Cartwright, *D.Phil Thesis* (Oxford, 1980).

7

Upper Limits for the Tau-Neutrino Rate

In this chapter, kinematic selection criteria are used to see if there is any indication of a significant tau-neutrino event rate. As we have seen that there is no visual confirmation of a tau-neutrino signal, the methods are used to set upper limits on the numbers of full density events and the fraction of prompt events which may be attributed to tau-neutrinos.

7.1 Introductory Remarks

7.1.1 Principles of kinematic tests

In formulating selection methods for ν_τ interactions, the essence of the problem is to discriminate between the leptonic tau decay process ($\nu_\tau N \to \tau X, \quad \tau \to l \nu_l \nu_\tau$) and the direct charged current production of the lepton l in the process ($\nu_l N \to l X$) and similarly, to discriminate between the hadronic tau decays ($\nu_\tau N \to \tau X, \quad \tau \to \nu_\tau +$ [hadrons]) and the neutral current process ($\nu_l\ N \to \nu_l +$ [hadrons]).

7.1.2 Kinematic tests for tau-neutrino interactions

There are several off-the-peg kinematic tests available which have been designed to enhance the number of tau-neutrino interations in a sample and reduce the background [1−3]. As our estimate shows, the number of ν_τ events is expected to be lamentably small and the signal to background ratio is never going to be very high. The various suggested search methods are discussed and the backgrounds and results are presented.

The methods are based on the effects of the different numbers of final state neutrinos in the processes which are compared, since these escape with a substantial momentum. We notice also that a majority of charged current tau-neutrino interactions have no visible charged lepton after the tau decay, and the ratio of apparent neutral to charged currents in our data will increase rapidly with the proportion of ν_τ induced events. This observation leads to the best experimental limit on the ν_τ event number (section 7.5).

7.2 General Procedure

7.2.1 Acceptances and backgrounds

To investigate the effectiveness of each method, we require a sample of simulated tau-neutrino data and a sample of data which represents what we expect to see in the absence of any tau-neutrino interactions (the background). For this purpose we have used data from WA59, a BEBC experiment which has the virtues of having used a wideband neutrino beam with an energy spectrum similar to the beam dump spectrum and $Ne - H_2$ as the detection medium. This is very important, as the effectiveness of the search methods depends critically on the accuracy of the momentum measurements in the liquid used.

For the tau sample, good muon events from WA59 are chosen in such a way as to reproduce the expected ν_τ spectrum in E_ν and y. The muon is replaced by a tau with the same momentum (rather than the same energy) as this avoids introducing an extra momentum imbalance which would affect the tests. The tau decay is then generated, and the decay products are added to the leptonic or hadronic momentum as appropriate. For the pure muon-neutrino sample, we select events which reproduce the observed muon-neutrino event spectrum. This treatment of the background and acceptance calculations automatically incorporates measuring errors and the effects of missing neutral particles in the final state in a consistent way for comparison with our data.

7.2.2 Statistical procedure for upper limits

We shall assume that the calculated errors on rates are Gaussian. The 90% confidence level upper limit for the measured rate is the value such that the cumulative probability in the physical region up to this limit is 90% of the total probability in the physical region. [4] The naïve calculation which sets the upper limit at the measured value plus 1.28 standard deviations gives unphysical results when the observed event rate is less than the expected background. In such a case we cannot ignore the fact that the background which actually occured must have fluctuated downwards from the calculated value.

7.3 Events with a final state Muon

7.3.1 Method

In a charged current muon-neutrino interaction, the final state particles consist of a muon and a hadron shower. In a plane perpendicular to the incoming neutrino beam we would expect the momenta of these particles to be balanced—within experimental error. For a tau decay to a muon and two escaping neutrinos, the observed momentum will not be balanced and this difference forms the basis of the Albright-Schrock test [1]. It should be noted that the larger number of neutral particles produced in electron-neutrino interactions and the measuring errors on the electron tracks themselves mean that such a test is not expected to produce significant results for the electron sample. The relevant variables are the missing momenta (i.e. the momentum vectors which would balance the observed momentum of an event) perpendicular to the beam direction ($\mathbf{p}_T^{miss}$) and normal to the production plane ($\mathbf{p}_p^{miss}$), and the angles between the hadron momentum and the muon and missing momenta in the plane perpendicular to the beam ($\Delta\phi_{\mu h}$, $\Delta\phi_{mh}$ respectively). Albright and Schrock proposed that the following steps be taken:

(i) Trigger on a single muon in the final state.

(ii) Apply standard experimental cuts on P_μ, E_ν (here $P_\mu > 3$ GeV, $E_\nu > 10$ GeV).

(iii) Look for events with significant $\mathbf{p}_T^{miss}$ and/or $\mathbf{p}_p^{miss}$ (> 1 GeV).

For the events selected the angular variables $\Delta\phi_{\mu h}$ and $\Delta\phi_{mh}$ are of interest, and they suggest

(iv) $\Delta\phi_{\mu h} \geq 90°, \Delta\phi_{mh} \geq 120°$

The distributions for the muon background and for the simulated tau sample were examined and the suggested cuts were found to be suitable. The $\mathbf{p}_T^{miss}$ and $\Delta\phi_{mh}$ distributions for muon-neutrinos, tau-neutrinos and the data are shown in figures 7.1–7.3, these variables being the ones which illustrate the greatest difference.

7.3.2 Results

When all the suggested cuts are applied to our data, 5 μ^- and 2 $\mu+$ events in the full density sample are selected. From the WA59 muons we would have expected 6.6 ± 1.1

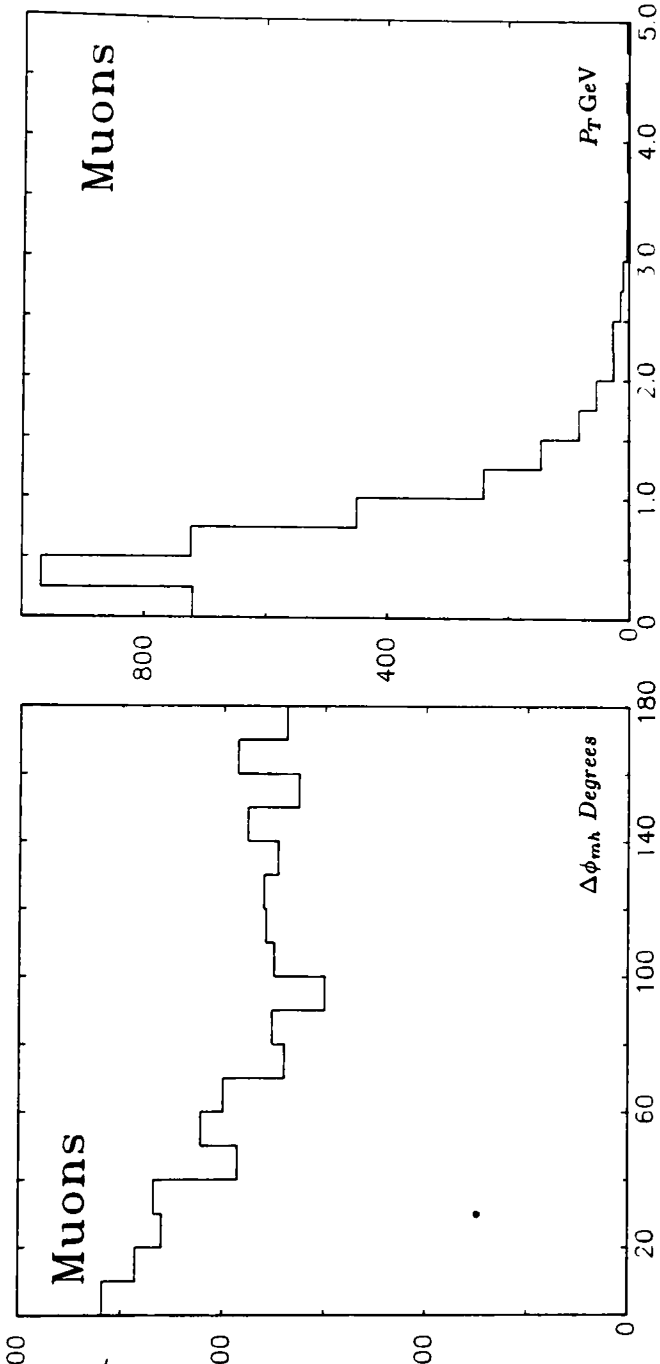

Figure 7.1 p_T^{miss}, $\Delta\phi_{mh}$ distributions—pure muon sample

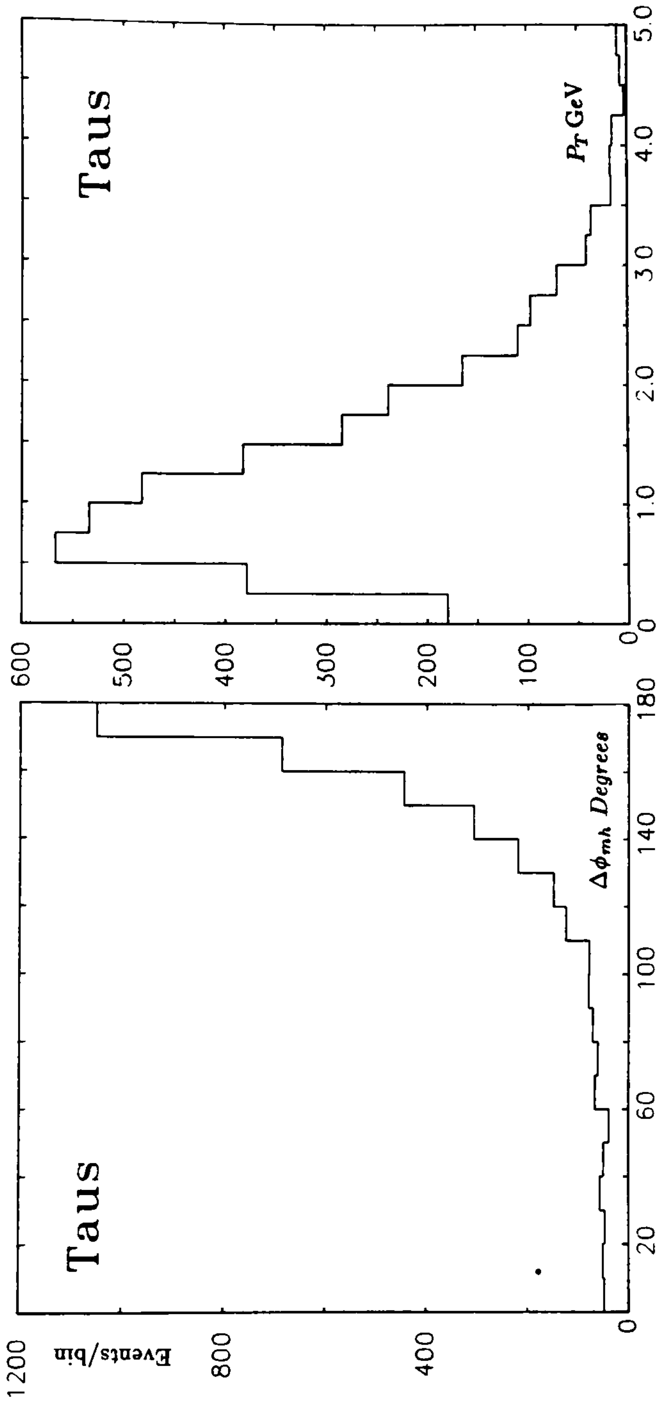

Figure 7.2 p_T^{miss}, $\Delta\phi_{mh}$ distributions—muons from tau decay

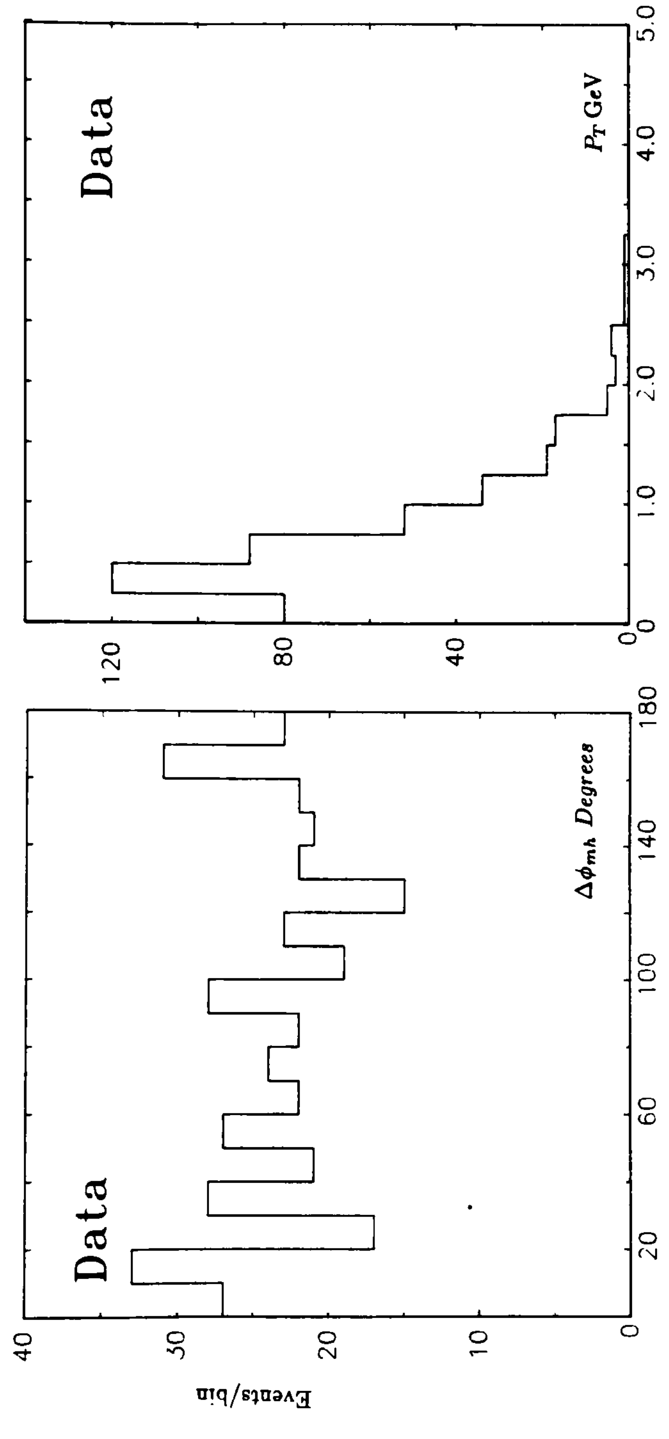

Figure 7.3 $\mathbf{p}_T^{miss}$, $\Delta\phi_{mh}$ distributions—data

and 1.4 ± 0.3 events respectively (normalising, of course, to the WA66 spectrum and muon event numbers). From the calculated tau decay signals $-1.6 \pm 2.5\,\mu^-$ and $0.6 \pm 1.4\,\mu^+$, the 90% CL. upper limits are then 2.1 observed μ^- and 2.6 μ^+ events. The acceptances calculated for $\tau^\pm$ decays into muons are 0.19 for τ^- and 0.17 for τ^+, giving the limit 26 events in full density altogether; adding the corresponding number of tau decays to electrons, this corresponds to approximately 22% of the prompt charged currents with $E_\nu > 10$ GeV.

7.4 Events with three charged pions and no lepton

7.4.1 Introduction

The method used in a Fermilab neutrino experiment [2] to search for tau-neutrino interactions (from oscillations) was applied to our data. The idea is to look for three charged pions from a hadronic tau decay, for which there is a 17% branching ratio. [5] Events are required to have no identified lepton, at least three charged pions with net charge ± 1 and invariant mass less than 1.8 GeV and one other particle. The visible momentum of the interactions must exceed 20 GeV as we shall see, and the background and acceptances are compared with the data by normalising the number of events which pass these basic cuts. We define $\mathbf{p}^T$ to be momentum transverse to the beam direction, $\mathbf{p}_3$ is the momentum of the selected three pion combination, $\mathbf{p}_{miss} = -\mathbf{p}_{vis}$ is the missing momentum and $\mathbf{p}_x = \mathbf{p}_{vis} - \mathbf{p}_3$ is the momentum of the remaining hadrons.

The cuts suggested are:

(i) $| \mathbf{p}_3 | > 20\,GeV$; $\quad | \mathbf{p}_3 | > 0.2 \; | \mathbf{p}_{vis} |$.

(ii) If $| \mathbf{p}^T_{miss} | > | \mathbf{p}^T_3 |$, require $(\mathbf{p}^T_3 . \hat{\mathbf{p}}^T_{miss}) > 1.0$ GeV.

(iii) If $| \mathbf{p}^T_{miss} | \leq | \mathbf{p}^T_3 |$, require $(\mathbf{p}^T_3 . \hat{\mathbf{p}}^T_x) < -1.5$ GeV.

(iv) The transverse momentum of the combination $| \mathbf{p}^T_3 |$ must exceed that of any other leaving track by at least 0.5 GeV.

(v) None of the three particles may be a leaving track with greater than 70% of the total momentum and 85% of the transverse momentum of the combination.

Details of the reasoning which led to this procedure may be found in the reference; its justification here will be the large acceptance for tau decays and small acceptance for neutral currents.

7.4.2 Acceptance calculation

Before proceeding, we check that the acceptance is reasonably high (c.f. the values ≈ 0.2 for the Albright–Shrock method). The acceptance for tau decays is calculated using the simulated tau data and modelling the tau decay to three pions assuming that this decay proceeds via the sequential 2-body decays $\tau \to A_1 \nu_\tau$, $A_1 \to \rho\pi$, $\rho \to \pi\pi$. The angular distributions in the hadronic decays are assumed to be of the form $d\Gamma \sim (1 - a\cos\theta)d\theta$

in the rest frame of the decaying hadron. The parameter a was set to $0, \pm 1$ for each decay to check that the exact choice is not important. The pion endtypes were chosen by approximating the distance d to the BEBC wall and assigning leaving endtypes with a probability $\exp(-d/d_{int})$, and the interaction length d_{int} was set to 60 cm, 1 m and 2 m to see what effect the endtype assignments had. The effect is not significant. The acceptance for the charged current tau-neutrino interactions with this decay mode for the tau is 0.288 for τ^- and 0.260 for τ^+, with a weighted average 0.28. This agrees with the Fermilab result (although they must assume a different energy spectrum) and with a result for this experiment generating the decays according to the phase space (and with $n = 4$ in the parametrisation of the F production).[6] It should be noted that our result is in fact an overestimate since we have not considered the decay $\tau \rightarrow 3\pi^{\pm}$, $2\pi^{\circ}$ which may contribute about half of the branching ratio to three charged pions. The two neutral pions from the tau decay will be included in the hadronic shower and clearly this will degrade the effectiveness of a method which relies on separating a clean three pion jet.

7.4.3 Signal and backgrounds

Two events in the full density sample pass the cuts. The momenta of the pions and the other hadrons in the plane transverse to the beam direction are shown in figure 7.4.

Backgrounds are expected from misidentified muons in the NC sample (considered separately for $P_\mu < 3$ and $P_\mu > 3$ GeV) and from some fraction of genuine neutral currents which pass the cuts. The background from misidentified muons with momenta above

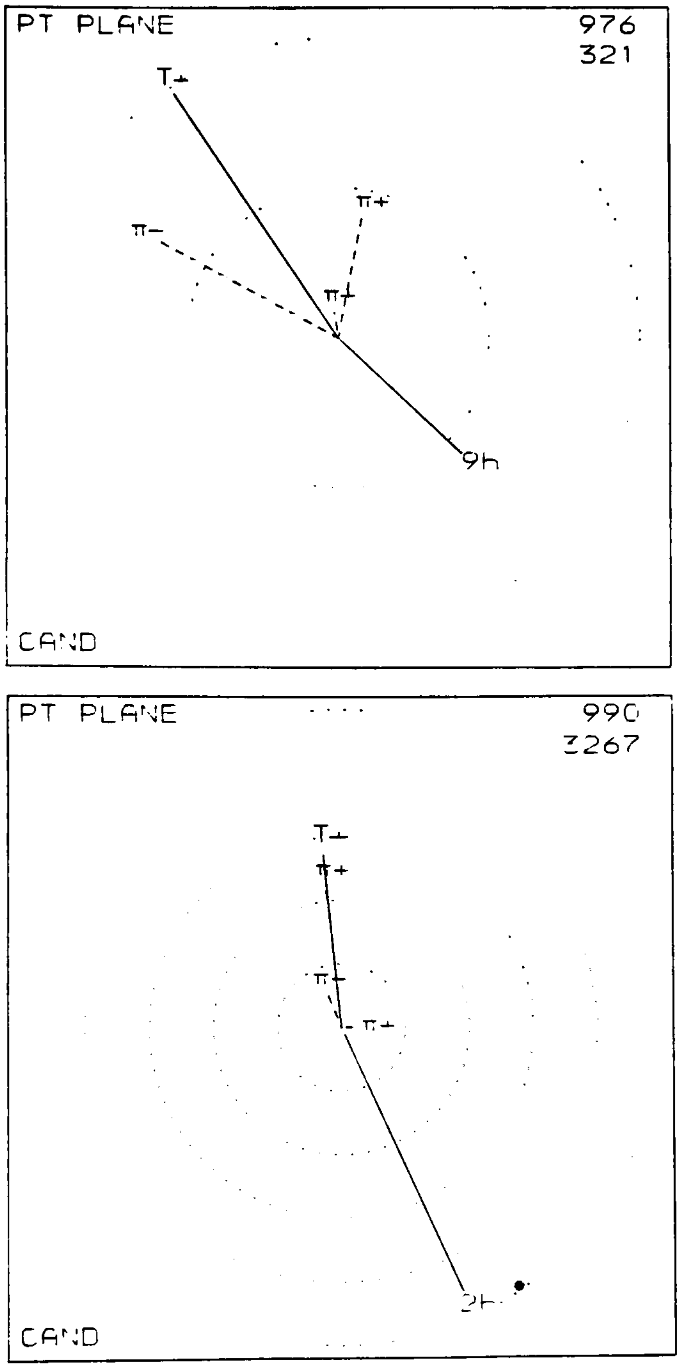

Figure 7.4 Tau decay to $3\pi^{\pm}\nu$: the selected event momenta in the plane perpendicular to the beam direction.
The circles show $| P_T | = 1, 2, 3 \ldots \mathrm{GeV}$
The $3\pi^{\pm}$ combination is labelled $\mathrm{T}^{\pm}$ for tau.

3 GeV is found using the WA66 events themselves and including the muon in the hadronic shower. The WA66 events are used for a good reason—if there is some fraction of muons from tau decay in the sample (and we cannot rule this out), these must be included in the background estimate here. Multiplying the number of events which pass the cuts by the probability of muon misidentification we expect 1.13 ± 0.60 events.

The number of misidentified low energy muons can be calculated assuming the standard y–distributions, but their effect here cannot easily be modelled. We assume that the fraction of events in the low energy sample which pass the cuts is the same as the fraction for high energy muons, provided we also approximate the fraction of low energy muons which are expected to have visible energy greater than 20 GeV. We expect a background 0.32 ± 0.07 events here. Misidentified electrons are neglected as we assume that the shower from the lepton harms the necessary resolution (but if the same fraction of electrons passed the cuts as muons we would add a further 0.8 ± 0.3 events background.)

The background in neutral events is calculated using hadron showers from WA59 charged current events and dropping the muon track. The events are selected to reproduce the hadronic energy spectrum seen in the WA66 neutral current sample. The calculation was done separately using μ^- and μ^+ events as a consistency check, giving backgrounds normalised to WA66 of 1.93 ± 0.94 and 4.41 ± 1.01 for μ^- and μ^+ origins respectively. The difference may possibly reflect a difference in multiplicity or charge balance. For our purposes we take the weighted mean 3.11 ± 0.70 events as the background.

7.4.4 Results

Subtracting all these background contributions from the data, our signal is -2.6 ± 1.7 events which gives a 90% CL. limit of 1.64 events. The acceptance calculation implies that the limit on tau decays to three pions is 5.9 events. Using the $\tau \rightarrow 3\pi^{\pm}\nu$ branching ratio, this corresponds to 34.7 charged current tau events in full density, or approximately 12.1 events in the charged current sample—approximately 5% of the prompt charged current signal above 10 GeV.

7.5 NC:CC Ratio and The Fraction of Tau-Neutrino Events

7.5.1 Introduction

As pointed out by Barger and Phillips[3], the apparent ratio of neutral to charged current events in a sample is very sensitive to the fraction of tau-neutrino events in that sample. It is assumed that the weak couplings for tau-neutrinos are the same as those for electron- and muon-neutrinos, i.e. universality, though as we shall see, the inclusion of the suppression for the charged current tau-neutrino events changes the neutral to charged cross-section ratio significantly. With their assumptions, the apparent ratio depends only on the branching ratio of the tau into leptons, and

$$R_{\tau} \approx \frac{R_{\mu} + (1 - \mathrm{BR}(\tau \rightarrow l\nu\nu))}{\mathrm{BR}(\tau \rightarrow l\nu\nu)}$$

where R_{μ} is the NC:CC ratio for muon-neutrinos. Using a 35% branching ratio for the leptonic tau decay and 0.35 for R_{μ}, the apparent NC:CC ratio for ν_{τ} interactions would be around 2.8, an order of magnitude greater than that for the other neutrinos. This estimate increases with the inclusion of the charged current suppression and with the requirement that events which include the tau decay products satisfy the experimental cuts which were applied to the data in section 3.8.

7.5.2 Procedure

We must calculate the ratio of neutral to charged current events for tau-neutrino events as they would appear in our corrected event numbers. To begin, if there is a fraction f of the total CC sample which comes from tau-decay, the apparent NC:CC ratio will be

$$R_{obs} = (1 - f)R_\mu + fR_\tau$$

and the fraction will therefore be given by

$$f = \frac{R_{obs} - R_\mu}{R_\tau \ - R_\mu}.$$

We use the measurement of R_μ from WA47,[7] a BEBC result for experimental conditions closest to ours. The cuts which were applied in order to obtain the ratio, apart from the standard cleaning-up variety, were a minimum hadron energy cut at 8 GeV visible energy (corresponding to 9.6 GeV corrected energy in our data) and a minimum hadronic momentum transverse to the beam direction of 1 GeV, the value which gave the minimum errors. For compatibility, the estimate of the apparent ratio for tau-neutrinos and the calculation for the experimental data have been based on the same cuts. The ratios obtained in all cases are not sensitive to the choice of R_μ value. The values R_{μ^-} =

0.345 ± 0.015 and $R_{\mu^+} = 0.364 \pm 0.029$ from WA47 give a value $R_\mu = 0.348 \pm 0.040$ for this experiment including the error on the ratio μ^+ to μ^-.

7.5.3 Apparent ratio for tau-neutrinos

To evaluate the ratio expected for the tau-(anti)neutrino sample, we use the simulated $\tau^\pm$ events. These samples include the effect of charged current suppression above threshold, so for every one of these events at an energy E_ν the number of neutral currents is given by the ratio R_μ scaled up by $\frac{\sigma(m_\tau \to 0)}{\sigma(m_\tau)}$. The expression for the expected ratio is

$$R_\tau = \int_0^{400} \frac{R_\mu(f(E_\nu, x)^{-1}) + \mathrm{BR}(\tau \to h\nu)^+}{\mathrm{BR}(\tau \to l\nu\nu)^+} dE_\nu$$

The integral over the event spectrum expected for tau-neutrinos is replaced by a sum over monte-carlo events in the calculation. The plus signs by the brackets showing the decay modes indicate that only those events which pass the experimental cuts are included. The ratio is then calculated by generating tau-neutrino interactions and tau lepton decays event by event and correcting these events exactly as if the final states were events in our data. This is of course the way in which any real tau-neutrino events in the real data would have been treated. The appropriate values of R_τ for comparison with the NC:CC ratio obtained in chapter 3 are 4.56 ± 0.46 for τ^- and 5.43 ± 0.53 for τ^+, with a combined ratio (weighting these values by the $\tau^+ : \tau^-$ event ratio calculated in chapter 5) 4.84 ± 0.35. The uncertainties in the value of R_μ, the leptonic branching ratio and statisitical limitations on the events generated contribute roughly equally to these errors. These results show that the Barger and Phillips test is more sensitive than the authors' original estimate.

7.5.4 Upper Limit on the Fraction of Tau-Neutrino Events

Collecting together the measured NC:CC ratio for WA66 full density events, the measured ratio for a pure muon sample (WA47) and the estimated ratio for tau-neutrino events, we find that the fraction of charged current events which can be attribute to tau-neutrino interactions is $-1.02 \pm 1.22\%$. The upper limit is 1.41% of charged current events with hadronic energy above 10 GeV in full density (4.5 events) which may be attributed to tau-neutrino interctions.

The upper limit for *all* events from tau-neutrinos is given by

$$F = \frac{R_{obs} - R_\mu}{R_\tau - R_\mu} \cdot \frac{1 + R_\tau}{1 + R_{obs}}$$

which we see is the fraction for charged currents multiplied by a factor which accounts for the relative proportions of neutral currents in the tau and data samples. The value $F = -3.4 \pm 9.3\%$ and the corresponding upper limit is 13% of full density events with hadronic energy greater than 10 GeV (roughly 76 events). Unfortunately it is not possible to express this limit as a fraction of *prompt* events without an additional assumption, as the prompt fraction in full density for $E_h > 10\,\mathrm{GeV}$ is 0.17 ± 0.19 by extrapolation and $0.16 \pm ^{.07}_{.06}$ by subtraction [8] (using the table in section 4 and integrating over the y-distributions to get the contribution above the hadronic energy cut). The uncertainty here being so large, we assume instead that the prompt fraction for $E_h > 10\,\mathrm{GeV}$ is the same as that for $E_\nu > 20\,\mathrm{GeV}$, 0.3. At the 90% confidence level, we cannot exclude a tau-neutrino source for 4% of prompt charged currents and 40% of the prompt events with $E_h > 10\,\mathrm{GeV}$.

References

[1] C.H.Albright and R.E.Shrock, *Physics Letters* **84B** (1979) 123.
C.H.Albright, R.E.Shrock and J.Smith, *Physical Review* **D20** (1979) 2177.

[2] H.C.Ballagh et al., *Physical Review* **D30** (1984) 2271.

[3] V.Barger and R.J.N.Phillips, *Physics Letters* **74B** (1978) 393.

[4] L.Lyons private communication.

[5] C.A.Blocker et al., *Physics Review Letters* **49** (1982) 1369.

[6] M.Talebzadeh, private communication.

[7] P.C.Bosetti et al., *Nuclear Physics* **B217** (1983) 1.

[8] J.Krstić, private communication.

Appendix 1

Tau Decays

The calculations of decay branching ratios for the tau lepton are summarised. V-A couplings for the weak interaction are assumed, which may be done since the available energy in the decays is well below the $W^{\pm}$ and Z° masses. The purely leptonic decay rates can be calculated with no further input, but the decays into hadrons ($u\bar{d}$ states) can only be calculated using experimental data to determine the weak couplings of the final state hadrons involved. The Cabbibo suppressed decays are not considered. References are not given in the text; each of the references given at the end cover much of this material and in greater detail than here.

(A) $\tau \rightarrow e\, \nu_e \nu_\tau$

The rate for this decay is given by the well-known expression for muon decay, with the tau lepton mass inserted in place of the muon mass, namely

$$\Gamma\left(\tau \rightarrow e\, \nu_e\, \nu_\tau\right) = \frac{G_F^2\, m_\tau^5}{192\, \pi^3}$$

and the distribution of neutrinos in angle and momentum is given by

$$d^3\, \Gamma \sim \left((3-2x) + (1-2x)\cos\theta\right)\; x^2\; dx\, d\, \cos\theta$$

where x is the energy of the ν_τ divided by its maximum allowed value of $\frac{m_\tau}{2}$.

(B) $\tau \rightarrow \mu\, \nu_\mu\, \nu_\tau$

If the muon mass is neglected, the rate is the same as for (A). The calculation with the muon mass taken into account leads to

$$\Gamma\left(\tau \rightarrow \mu\, \nu_\mu\, \nu_\tau\right) = \Gamma\left(\tau \rightarrow e\, \nu_e\, \nu_\tau\right)\left(1 - 8y - O(y^2)\right),\quad y = \frac{m_\mu^2}{m_\tau^2} \approx 0.97\Gamma(e)$$

It is interesting to note that the current measurements show that the decay to a muon is preferred (though the difference is hardly significant statistically).

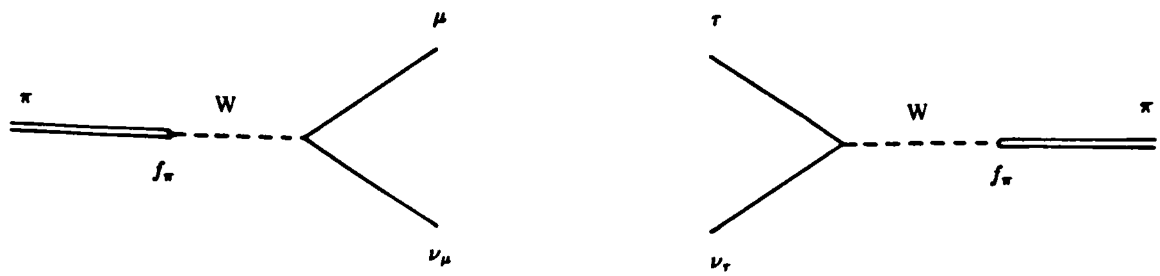

Figure A1
Diagrams for the decays $\pi \to \mu\nu$, $\tau \to \pi\nu$

(C) $\tau \to \pi \, \nu_\tau$

The pion coupling to the axial current is known from the pion decay process $\pi \to \mu \, \nu_\mu$ (B.R. ~ 100%). This is exactly the coupling required for this tau decay mode, which can be seen by comparing the diagrams for the two processes (figure A1). From pion decay $f_\pi \approx 0.94\, m_\pi$, and the hadronic current is $f_\pi \, q_\pi^\alpha$. The rate can then be calculated and the result is

$$\Gamma(\tau \to \pi \, \nu_\tau) = \frac{G_F^2 \, f_\pi^2 \, m_\tau^3 \cos^2\theta_c}{16\pi} \left(1 - \frac{m_\pi^2}{m_\tau^2}\right)$$

$$d\Gamma \sim (1 - \cos\theta) d \cos\theta$$

$$\cos\theta = \hat{\mathbf{p}}_\pi . \hat{\mathbf{s}}_\tau$$

(D) $\tau \rightarrow \rho \, \nu_\tau$

The coupling of the ρ-meson in the weak process is obtained using the idea of conserved vector current (CVC) which means that we may replace its coupling e in the electromagnetic interactions by $\sqrt{2} g \cos\theta_c$, $(g^2 = \frac{M_W^2 G_F^2}{\sqrt{2}})$. Using the process $e^+ e^- \rightarrow \rho^\circ$, the electromagnetic coupling is parametrised as

$$\Gamma(e^+ \, e^- \rightarrow \rho_\circ) = \frac{4}{3} \, \pi \, \alpha^2 \, \frac{m_\rho}{\gamma^2}$$

and the corresponding expression for tau decay is then

$$\Gamma(\tau \rightarrow \rho \, \nu_\tau) = \frac{G_F^2 \, \cos^2\theta_c}{8 \, \pi \, \gamma^2} (1+R)^2 \, (1+2R), \quad R = \frac{m_\rho^2}{m_\tau^2}$$

the results for $\frac{\gamma^2}{4\pi} = 2.36$ are

$$\Gamma(\rho) = 1.3 \, \Gamma(e)$$

$$d\Gamma \; \sim \; (1 + a h \cos\theta) \, d\cos\theta, \quad a = \frac{m_\tau^2 - 2m_\rho^2}{m_\tau^2 + 2m_\rho^2} \approx 0.46, \quad h = \text{helicity}$$

(E) $\tau \rightarrow A_1 \nu_\tau$

For this mode the Weinberg sum rules, which relate the axial and vector coupling strengths, are used together with the identification of the vector part of the coupling with the ρ alone and the axial part with the A_1. The value of γ for the A_1 is then related to that for the ρ used in section (D) by

$$\frac{m_{A_1}^4}{\gamma_{A_1}^2} = \frac{m_\rho^4}{\gamma_\rho^4}$$

and we find

$$\Gamma(A_1) \approx 0.37\,\Gamma(\rho)$$

(F) $\tau \rightarrow 4\pi\, \nu_\tau$

This decay, like that of the rho, can be related via the CVC hypothesis to the process $e^+ e^- \rightarrow 4\pi$ where the 4-pion final state has net charge zero. Assuming isospin symmetry gives the appropriate coupling for a charged 4-pion state. The rate is expected to be dominated by the $\rho'(1600)$ resonance, and we assume that this two body decay mode gives the correct neutrino energy. The expected rate for this mode is $\Gamma(4\pi) \approx 0.33\Gamma(e)$.

References

Y.S.Tsai, *Physical Review* **D4** (1971) 2821.

H.B.Thacker and J.J Sakurai, *Physics Letters* **36B** (1971) 103.

J.Augustin, *Proceedings of LEP summer study* (Les Houches and CERN, 1978).

L.B.Okun, *Leptons and Quarks* (North-Holland, 1982).

F.J.Gilman and Sun Hong Rhie, SLAC–PUB–3444 (1984).

Appendix 2

The WA66 Collaboration

H.Grässler
III Physikalishes Institut der Technischen Hochschule, Aachen, W. Germany

W.Dröge, U.Idschok, H.Kreutzmann, B.Nellen and B.Wünsch
Physikalisches Institut der Universität Bonn, Bonn, W. Germany

A.M.Cooper–Sarkar, D.C.Cundy, H.Foeth, A.Grant, H.Klein, D.R.O.Morrison, M.Nikolić, L.Pape, M.A.Parker, P.Schmid and H.Wachsmuth
CERN, Geneva, Switzerland

M.Dris, E.Simopoulou and A.Vayaki
Demokritos Nuclear Research Centre, Athens, Greece

K.W.J.Barnham, D.B.Miller, M.M.Mobayyen and M.Talebzadeh
Imperial College of Science and Technology, London, UK

M.Aderholz and W.Wittek
Max Planck Institut für Physik und Astrophysik, Munich, W. Germany

P.Bostock, G.Myatt and J.Krstić
Department of Nuclear Physics, Oxford University, Oxford, UK

J.Guy and W.Venus
Rutherford Appleton Laboratory, Chilton, Didcot, UK

T.Bolognese, M.L.Faccini–Turluer and D.Vignaud
DPhPE, CEN Saclay, Gif-Sur-Yvette, France

P.O.Hulth, K.Hultqvist and Ch.Walck
Department of Physics, University of Stockholm, Stockholm, Sweden